Accepted Manuscript

Please cite this article as: Y-T. Zhang, M.S. Alber, S.A. Newman, Mathematical Modeling of Vertebrate Limb Development, *Mathematical Biosciences* (2012), doi: http://dx.doi.org/10.1016/j.mbs.2012.11.003

Mathematical Modeling of Vertebrate Limb Development

Yong-Tao Zhang[1],*, Mark S. Alber[1,2],*, Stuart A. Newman[3],*

[1]Department of Applied and Computational Mathematics and Statistics, University of Notre Dame, Notre Dame, IN 46556, USA

[2]Department of Medicine, Indiana University School of Medicine, Indianapolis, IN 46202 USA

[3]Department of Cell Biology and Anatomy, Basic Science Building, New York Medical College, Valhalla, NY 10595, USA

*Corresponding authors. Emails: malber@nd.edu (M.S. Alber), newman@nymc.edu (S.A. Newman), yzhang10@nd.edu (Y.-T. Zhang).

Abstract

In this paper, we review several main mathematical and computational models of vertebrate limb development and their roles in accounting for different aspects of this process. The main aspects of limb development have been modeled, including outgrowth and shaping of the limb bud, establishment of molecular gradients within the bud, and formation of the skeleton. These processes occur interdependently during development, although (as described in this review), there are various interpretations of the biological relationships among them. A wide range of mathematical and computational methods have been used to study these processes, including ordinary and partial differential equation systems, cellular automata and discrete, stochastic models, finite difference methods, finite element methods, the immersed boundary method, and various combinations of the above. Multiscale mathematical modeling and associated computational simulation have become integrated into the study of limb morphogenesis and pattern formation to an extent with few parallels in the field of developmental biology. These methods have contributed to the design and analysis of experiments employing microsurgical and genetic manipulations, evaluation of alternative hypotheses for limb bud outgrowth, interpretation of the effects of natural mutations, and the formulation of scenarios for the origination and evolution of the limb skeleton.

1. Introduction

The development of the vertebrate limb is one of the best studied examples of multicellular organogenesis (Tickle, 2003; Newman and Müller, 2005; Newman and Bhat, 2007). The process involves outgrowth from the body wall of tetrapods (i.e., amphibians, reptiles, birds, mammals: vertebrates other than fish) of two pairs of *mesenchyme* (embryonic connective tissue) masses covered by a specialized *ectoderm* (embryonic skin, continuous with the rest of the body surface). All tetrapod limbs contain *endoskeletons* composed of rods and nodules of cartilage or bone, separated by discontinuities, or joints. Thus, understanding limb development involves addressing two main problems: that of limb bud outgrowth and shaping and that of skeletal pattern formation (Fig. 1).

The outgrowth and shaping problem lends itself to mathematical and computational modeling that takes into account the physical properties of the involved tissues (reviewed in Hopyan et al., 2011). The limb bud mesenchymal mass – the *mesoblast* – is a deformable viscoelastic material that is immiscible with the surrounding flank mesenchyme when it first emerges from the body. Its constituent cells can change the mesoblast size and shape by dividing either isotropically or directionally, and they can intercalate among one another, stretching and distorting the tissue mass. Surrounding the mesoblast is an epithelial sheet underlain by an acellular basement membrane, both with mechanical properties of their own. The epithelium is also the source of molecular signals that induce and modulate the cellular behaviors of the underlying mesenchyme.

The endoskeletons of all vertebrate limbs exhibit repetitive motifs and are variations on a common morphological theme, so understanding their generation is particularly well-suited to mathematical models in which a generic skeletogenic mechanism can be hypothesized and its parameters varied according to plausibly variant developmental scenarios. The nature of the patterns, and of experimental results on skeletal patterning of randomized limb mesenchymal cells in vivo and in vitro, have led to most such models being based on the physics of self-organizing

systems (e.g., Turing-type reaction-diffusion processes) applied to the molecular biology of cell-cell and cell-ECM interactions (reviewed in Newman et al., 2008).

A different view of skeletogenesis, which has been influential over the past four decades, treats the skeletal pattern as a downstream readout by the cells' genomes of spatial coordinates, the values of which are specified by graded concentrations of, or duration of exposure to, "positional information" (PI) molecules (Wolpert, 1971; Summerbell et al., 1973; reviewed in Towers and Tickle, 2009). Here the generic aspects of the final pattern (i.e., the quasi-periodic arrangement of the discrete elements), is ignored. The establishment and dynamics of the monotonic positional gradients in this PI framework are also amenable to mathematical modeling (see below). There is increasing recognition based on experimental tests, however, that the spatial patterns in question, usually of diffusible morphogen molecules and Hox and related transcription factors, are not sufficient to account for the actual features of the skeletal pattern without including the self-organizational properties of the limb mesenchyme (see, e.g., Wolpert and Tickle, 2010). Most likely the PI gradients fine-tune the details of the skeletal elements during their formation (Tamura et al., 2011).

Although limb bud outgrowth and shaping are thus conceptually separate problems from the formation of the skeleton, some of the molecules that control skeletogenesis also influence outgrowth and shaping (Newman and Müller, 2005). Limb bud shape and its developmental transformation also influence the outcomes of proposed skeletogenic mechanisms. For example, in small spatial domains such as limb bud, the spatial patterns resulting from reaction-diffusion and related self-organizing processes are strongly influenced by the domains' boundary conditions, size, and shape (Borckmans et al., 1995; Zhu et al., 2009a; 2009b; 2010).

In what follows we first present a brief biological background and then describe the main models that have been used to characterize limb bud growth and shaping, and the generation of molecular gradients in the mesoblast. Next we present a detailed description of models employing self-organizing dynamics of skeletal patterning in vitro and in vivo. In the concluding section we discuss the prospects for

bringing together the various mathematical and computational approaches reviewed here. In particular, we will describe the general form of a comprehensive model that includes a self-organizing skeletogenic component that evolves in developmental time in the context of an autonomous limb bud growth and shaping mechanism, and whose generated skeletal elements are customized by the local concentrations of dynamically changing PI morphogens and transcription factors. A comprehensive review of limb development models has recently appeared (Glimm et al., 2012), which in contrast to this contribution is directed primarily towards a non-mathematical audience.

2. Biological Background

Limb bud outgrowth and shaping

The limb emerges from the embryonic body wall, or flank, under the influence of a diffusible morphogen, fibroblast growth factor 8 (FGF8), secreted by the ectoderm overlying the prospective limb mesenchyme. In birds and mammals, as outgrowth proceeds, a thickened ridge of ectoderm running anteroposteriorly (AP axis: thumb to little finger) along the limb bud tip, the apical ectodermal ridge (AER), forms and serves as the source of the FGF8. Early effects of FGF8 are to transform the prospective limb mesenchyme into a more cohesive and mechanically active material than the flank mesenchyme from which it is derived (Damon et al., 2008). This has been suggested to be responsible for its "phase separating" from the adjacent flank, rounding up, and propelling itself forward (Damon et al., 2008).

Factors secreted by the AER, including FGF8, are also responsible for keeping the mesenchyme of the limb tip in a developmental labile state, primarily by suppressing its capacity to condense (see below) and differentiate into cartilage (Kosher et al., 1979). Cartilage is not easily reshaped, so the main determinants of limb shaping act at the distal (distant from the body) end of the developing limb, even as the more proximal (close to the body) regions are undergoing chondrogenesis. This results in a proximodistal (PD) temporal sequence of development. Factors that

regulate the formation of the AER and its AP length (discussed in the subsection on *non-skeletally-isomorphic patterns*, below), are indirectly involved in limb bud shaping. In addition, biologically plausible mechanisms of the spatiotemporal development of the skeleton (discussed in the subsection on skeletal pattern formation, below), must incorporate the suppressive effect of the AER.

After the limb bud has emerged, its outgrowth and shaping are the result of the behaviors of the mesenchymal cells in the context of the surrounding ectoderm. Here the morphogens secreted by the ectoderm are also important. For many years the standard view was that the effect of the morphogens, FGFs in particular, were mitogenic, i.e., promoting cell division, and that limb bud outgrowth resulted from a proliferation gradient with its maximal value at the distal tip. Some of the mathematical models of outgrowth and shaping described in the following section are based on this biological mechanism. Recent work, however, has shown that the mesenchymal cells of the limb bud exhibit a chemotactic migratory response to FGF gradients (Li and Muneoka, 1999) and oriented movement and growth (Boehm et al., 2010; Wyngaarden et al., 2010). The orientation of the cells is dependent on Wnt signaling, while FGF signaling affects cell velocity (Gros et al., 2010). Limb mesenchyme may also exhibit oriented convective flow, as seen in gastrulating mesoderm (Zamir et al., 2006) (see Hopyan et al., 2011, for a review of oriented cell behaviors in the developing limb). These new findings are increasingly being incorporated into mathematical models of limb outgrowth and shaping.

Some models have considered the possibility that the dorsal and ventral ectoderm act as a mechanical constraint that guides the flow of the limb mesenchyme. While there is some evidence for such a role for the ectoderm (Borkhvardt, 2000), there are also studies indicating that the dorsal ectoderm (though possibly not its underlying basement membrane) in not absolutely required for normal limb shaping (Martin and Lewis, 1986).

Non-skeletally-isomorphic patterns of morphogens and other molecules

The original formulation of the PI concept suggested that the AP, and PD axes,

described above, and the dorsoventral (DV: back to front) axis defined a coordinate system of molecules that were interpreted by the mesenchymal cells so as to assume their position-specific fate (Wolpert, 1969). The PI molecules were specifically postulated to be non-isomorphic to the developing or final limb skeletal patterns. That is, they were proposed to serve an informational (i.e., eliciting portions of the pattern that are hypothesized to be independently encoded in the genome) rather than a prepatterning role (Wolpert, 1969).

It soon became clear that the limb axes are not specified independently of each other (Bowen et al., 1989), that the putative molecular determinants of the axes are mutually regulatory (Laufer et al., 1994; Yang and Niswander, 1995), and that some are indeed dispensable for the generation of the basic skeletal pattern (Litingtung et al., 2002). The specification of skeletal pattern by positional information is also inconsistent with evidence that quasi-periodic limb-like skeletons can form from dissociated, randomized mesenchymal cells repacked into ectodermal hulls (Zwilling, 1964; Ros et al,, 1994). Nevertheless, the assumption that the major features of the skeletal pattern are set by cells' exposure to continuous, non-skeletally isomorphic, fields of diffusible molecules produced by signaling centers oriented according to the three classical anatomical axes remains a popular theme in models of limb development (e.g., Bénazet and Zeller, 2009; Towers et al., 2012, citing Meinhardt, 1978).

In any case, experimental and theoretical studies on the generation of gradients of non-skeletally-isomorphic morphogens and non-diffusible molecules (such as Hox transcription factors) in the developing limb continue to be of significance. This is because, as mentioned above, such factors are important determinants of limb outgrowth and shaping (which indirectly affects the number, size and shape of the skeletal elements that form within the growing bud), and also because the presence of different concentrations of these factors, for various durations, during chondrogenesis, influences the character of elements formed, fine-tuning and customizing the skeletal structures (see, e.g., Tamura et al., 2011).

Key signaling centers for establishing these gradients are the AER, mentioned

above as the major source of FGF8, and the zone of polarizing activity (ZPA), the limb bud's major source of the morphogen Sonic hedgehog (Shh). The AER is essential for limb outgrowth, shaping and skeletogenesis (Saunders, 1948). Sonic hedgehog was thought to be the AP positional information determinant, but its absence (along with a transcriptional regulator of its function, Gli3) actually leads to increased numbers of digits via the impairment of its role in limb bud shaping (Litingtung et al., 2002). This indicates that Shh is a modulator of skeletogenesis rather than part of its core generative mechanism.

A recent integrative description of the interplay among signaling centers responsible for gradient systems in the developing mouse limb postulates feedback loops involving the morphogens FGF, Shh, Wnt and bone morphogenetic factor 4 (BMP4), and Hoxd-class, Gli3 and Hand2 transcription factors (Zeller et al., 2009). This model is relevant to the demonstrated roles of these gradients in the maintenance and localization of the AER and ZPA, notwithstanding its underlying assumption that they determine the skeletal pattern according to the PI framework. Indeed, like other PI-based models, that of Zeller et al. (2009) does not attempt to account for the actual placement of skeletal elements.

Skeletal pattern formation

Initially the mesenchymal cells of the limb mesoblast are distributed uniformly within an ECM rich in the polysaccharide hyaluronan. Before these cells differentiate into chondrocytes, they transiently condense into tight aggregates at discrete sites where the cartilaginous elements will ultimately form. Precartilage condensations (and before them, more subtle proto-condensations), form when the ECM changes locally in composition, first becoming richer in the glycan binding proteins known as galectins (Bhat et al., 2011) and later in glycoproteins such as fibronectin. These aggregations are further consolidated through cell-cell adhesive interactions mediated by cell-surface attachment molecules (CAMs) such as N-CAM (Widelitz et al., 1993), N-cadherin (Oberlender and Tuan, 1994), and possibly cadherin-11 (Luo et al., 2005).

All the precartilage mesenchymal cells of the limb mesoblast are capable of

producing the skeletogenic ECM molecules and CAMs but only those at sites destined to form skeletal elements do so. There must be communication among the cells to divide the labor in this respect. Galectins can act as morphogens as well as adhesion molecules (reviewed in Gabius, 2010) and one of these molecules, CG (chicken galectin)-1A, plays both roles in the avian limb bud earlier than any other known factors (Bhat et al., 2011). Another galectin, CG-8, is part of a mutually excitatory loop with CG-1A at the level of gene expression, but antagonizes the latter's condensation activating activity at the protein interaction level (Bhat et al., 2011). Later in the chondrogenesis pathway diffusible factors of the TGF-β family are produced. These promote the production of fibronectin (Leonard et al., 1991) and cadherins (Tsonis et al., 1994) and positively regulate their own synthesis in limb bud mesenchyme (Miura and Shiota, 2000a).

Although the AER is a unique source of a particular outgrowth-promoting subset of FGFs, the entire limb ectoderm produces morphogens of this class (Mariani and Martin, 2003). The FGFs produced by the ectoderm affect the developing limb tissues through three distinct FGF receptors. The cells of the apical zone express FGF receptor 1 (FGFR1) (Peters et al., 1992; Szebenyi et al., 1995). Signaling through this receptor presumably mediates the suppressive effect of the AER in this region of the developing limb. As the chicken limb elongates, cells begin to condense at discrete foci, but only at a sufficient distance (~0.3 mm) from the AER. Cells at sites of incipient condensation express FGFR2 rather than FGFR1 (Peters, et al., 1992; Szebenyi et al., 1995; Ornitz and Marie, 2002; Moftah et al., 2002). Activation of these FGFR2-expressing cells by FGFs induces a laterally-acting (that is, peripheral to the condensations) inhibitory effect which suppresses cartilage differentiation (Moftah et al., 2002). Signaling via the Notch pathway, which is initiated by cell-cell contact, also plays a part in this lateral inhibitory effect (Fujimaki et al., 2006).

The result of the pattern-forming process is that a stereotypical arrangement of first, cartilage elements, and then the bones that replace them in most tetrapod species, emerge in a proximodistal fashion. Almost invariably there is one element (the humerus or femur, referred to generically as the "stylopod") attached to the body,

two elements (the radius and ulna, or tibia and fibula: the "zeugopod"), and a species- or limb type-characteristic number of wrist elements, followed by fingers or toes (the "autopod").

This summary indicates that the limb bud mesenchyme is subject to a variety of intrinsic and extrinsic interactions that have both activatory and inhibitory effects on precartilage condensation and chondrogenesis. Collectively these cellular and molecular interactions constitute a core mechanism for the generation of the cartilaginous primordia of the limb skeleton. Several of the models described in the following section explicitly incorporate these processes, characterizing parameter choices and other conditions under which biologically realistic skeletal patterns are formed.

3. Mathematical Models

Models primarily involving growth and shaping of the limb bud

Dillon and Othmer (1999; reviewed in Dillon, 2001) presented a continuum mathematical and computational model coupling fluid flow and elastic boundaries (the immersed boundary method; Peskin, 2002), to describe limb bud growth in 2D. They provided one of the first computational tools for exploring the effects of mutations and experimental interventions on the relation of gene expression patterns and growth in the developing limb. The model incorporates the effect of morphogens (i.e., FGFs and Shh) with sources at the AER and the ZPA, the dynamics of which are governed by reaction-diffusion-advection equations. Since spatiotemporal profiles of these factors are generated in the model and contribute to growth and shaping of the bud (the proximodistal gradient of FGF is suggested to induce a gradient of cell division, for example), the model can also be considered in the class (described below) dealing with the generation of morphogen patterns that are non-isomorphic to the skeleton.

In the Dillon-Othmer model a viscous fluid domain of constant density representing the limb bud mesoblast is surrounded by a moving boundary incorporating the mechanical and biochemical properties of the ectoderm. The fluid

motion is described by the Navier-Stokes equations

$$\nabla \cdot v = U(c, x, t),$$
$$\rho \frac{\partial v}{\partial t} + \rho(v \cdot \nabla)v = -\nabla p + \mu\left(\nabla^2 v + \frac{1}{3}\nabla U\right) + \rho F. \qquad (1)$$

Here U is the local source strength for growth which depends on morphogens c_1 and c_2 (c for simplicity), the location x of the tissue within the limb bud and the age t of the limb. The variable v is the fluid velocity, ρ is the fluid density, p is the pressure, and μ is the fluid viscosity. The term F is the force density that limb bud ectoderm exerts on the fluid surrounding it. The evolution of the morphogens is modeled by a reaction-diffusion-advection system

$$\frac{\partial c}{\partial t} + \nabla \cdot (vc) = D\nabla^2 c + R(c). \qquad (2)$$

D is the diffusion matrix for the morphogens and $R(c)$ is the production rate. The Dillon-Othmer model was unique in its consideration of the relationship between growth as a physical process, the potential effects of morphogens on the parameters of growth, and the objective of reconciling empirically measured shapes and growth rates distributions of identified morphogens during the course of development. While some of the physical and biological assumptions of the model have been reevaluated in light of new information (see below), it (along with the extension by the same group (Dillon et al, 2003; see below)) remains the only one to date to integrate the two main non-skeletogenic processes.

In a later 2D treatment, Murea and Hentschel (2007) studied limb outgrowth as a free boundary problem, controlled by a creeping flow of the expanding mesoblast with a nutrient-driven volume source and an ectodermal boundary with nonuniform surface tension. Unlike in Dillon and Othmer (1999), no assumption was made concerning a proximodistal gradient of mitoses, a departure that was later validated empirically (Boehm et al., 2010; see below). The authors also suggested that the high viscosity

and low Reynolds number of the mesenchyme justifies, rather than the full Navier-Stokes equation, the use of the simpler Stokes equation

$$-\mu\Delta v + \nabla p = f + \frac{\mu}{3}\nabla S .$$ (3)

Here p is a pseudopressure field or "tissue pressure," defined by $p = P - p_{air}$, where P is the pressure of the fluid and μ is the viscosity of the fluid. The gradient of p yields the velocity of the limb bud's outgrowth.

A novel finite element algorithm was developed to deal with a free boundary in nonconvex domains (i.e., the proximal portions of the growing bud, which have straight anterior and posterior edges). The introduction of a variable surface tension in the ectoderm (a lower value at the tip) ensures that the limb bud expands in a proximodistal direction rather than ballooning out. This is a biologically plausible solution to this problem (see Borkhvardt, 2000), which in the model of Dillon and Othmer (1999) was implemented by the ad hoc elastic tethering of opposite points on the ectoderm.

Morishita and Iwasa (2008) explored the potential of a discrete model of "growth-based morphogenesis" to describe changes of organ morphology during limb development. Like the fluid mechanics-based model described above, this discrete model describes the growth of the vertebrate limb bud as an interaction between tissues with different physical properties. The model represents the mesenchyme and epithelium each by a network of nodes, denoted respectively as M- and E-nodes. To model the dynamics of the AER, a key component in regulating limb outgrowth, the authors used the following reaction-diffusion equation defined on the nodal network:

$$c_i^M(t+dt) = c_i^M(t) + D\left\{\sum_j\left(c_j^M(t) - c_i^M(t)\right) + \sum_k\left(c_k^{AER} - c_i^M(t)\right)\right\}dt - \gamma c_i^M(t)dt.$$ (5)

c_i^M is the AER-signal concentration at the M-node i, c_k^{AER} is the AER-signal concentration at the E-node k of AER. The AER signal is assumed to diffuse only between linked nodes with a diffusion constant D. The chemical flux at each node is proportional to the difference between the focal node and its neighbors. The first

summation term includes all M-nodes j linked with the node i, and the second summation includes all E-nodes k linked with the node i. c_k^{AER} is assumed to be constant. γ is a degradation rate of the AER-signal at each M-node.

By running model simulations under their growth-based morphogenesis assumption (which has recently been questioned; see below), the authors concluded that: (1) the ratio of limb bud length to limb bud width is determined by the spatial pattern of volume sources realized through cell proliferation in the mesenchyme; (2) elastic balance between mesenchyme and epithelium is required for normal morphogenesis; (3) normal elongation of limb bud is not observed if the domain with high proliferation activity does not dynamically change with the growth and deformation. Compared to the viscous flow/FEA approach, the adaptivity and simple computational implementation of this discrete model make it useful in analyzing the control of organ morphology by the spatiotemporal pattern of volume sources.

Boehm et al. (2010) presented a fluid dynamics model (like Dillon and Othmer, 1999 and Murea and Hentschel, 2007), but in 3D, using a finite element computational approach (like Mura and Hentschel, 2007). The model employs the Navier-Stokes equations to represent the mesenchyme as a viscous incompressible fluid whose volume increases corresponding to s, a distributed source term (as used in the earlier two models), representing the patterns of cell division, for which a set of new data were provided. As in Hentschel and Murea (2007), omission of the convection term was justified by the high viscosity of the limb bud mesenchyme:

$$
\begin{aligned}
&\frac{\partial v}{\partial t} + \nabla p - \frac{1}{\mathrm{Re}} \nabla \cdot [\nabla v] = 0, \\
&\nabla \cdot v = s,
\end{aligned}
\tag{4}
$$

where v is velocity, p is pressure, and Re is the Reynolds number. The source term s was directly calculated from the new atlas of cell cycle times.

Numerical simulations, supported by new measurements and parameter optimization, suggest that contrary to long-held assumptions, local sources of

isotropic proliferation were not sufficient to account for the shape of the growing limb bud (a feature not only of the models of Dillon and Othmer, 1999 and Morishita and Iwasa et al., 2008, discussed above, but also of the cellular automata-based limb bud shaping model of Poplawski et al., 2007). An example of the simulations of Boehm et al. (2010) is shown in Fig. 2. The limb mesoblast is represented as an incompressible fluid with a distributed source term, *s* representing the patterns of cell division. The final growth pattern (A) shows a discrete region of very high proliferation at the distal tip (red/yellow) and shrinking areas dorsal and ventrally (blue). The resulting tissue displacements (B) generate a shape (green surface in C, D) which shows a good correspondence to the real shape (blue in D), but only for a distribution of proliferation rates in conflict with experimental values.

The authors thus concluded that directional cell activities (i.e., oriented cell division, as well as oriented cell motility; Wyngaarden et al., 2010), not incorporated in these simulations, are likely to be the driving forces for limb outgrowth. This theoretical prediction led to the discovery of a highly branched and extended cell shape composed of dynamically extending and retracting filopodia and a distally oriented bias in Golgi position, as well as a bias in the orientation of cell division (Boehm et al., 2010).

An integrated view of the newly appreciated role of directional activities in limb bud outgrowth, including the tissue-level expulsive forces generated by the mechanically excitable flank acting on the forming limb bud (Damon et al., 2008), is presented by Hopyan et al. (2011).

Models primarily involving dynamics of morphogens non-isomorphic to the skeleton

No evidence has ever been found for a genomic representation of the limb skeletal pattern that would permit non-isomorphic distributions of morphogens, or duration of exposure to them, to be interpreted in a cell-autonomous fashion so as to differentiate into spatially appropriate portions of the skeleton. Nonetheless, the assumption that such an interpretive mechanism exists (as required by the PI model), has motivated many experimental studies tracking the spatiotemporal dynamics of candidate PI

morphogens, as well as several mathematical and computational models of these dynamics.

An early example of such work is found in two papers by Meinhardt (Meinhardt, 1983a,b). The model addressed a number of issues in limb developmental biology, such as the positioning of the limbs along the body axis and the regeneration of limb structures in urodele (tail-bearing) amphibians, both outside the scope of this Review, but also the development of the limb skeleton, which is within our range of topics. The novel concept of this paper, which was applied to each of the developmental problems, is the formation of new structures, including gradient sources, at the interface of two or more distinct tissues or populations of cells. Meinhardt calls this a "boundary model" to contrast it with the "gradient hypothesis" proposed by the developers of the PI idea (Tickle et al., 1975). In the latter, each cell's positional identity is determined by the local values of two chemical concentrations or exposure-duration gradients, whereas in the former, the direct confrontation of independently induced cell populations set up gradients unrelated to the determinants of the original tissues, which modulate the further spatially nonuniform development of one or both of the interacting cell types (Meinhardt, 1983a).

The Meinhardt boundary model has proved useful in accounting for the properties of several developmental systems (reviewed in Meinhardt, 2008), despite the lack of experimental support for notion that gradients purportedly established by this mechanism in the limb are used as positional information to specify locations of skeletal elements. Non-skeletally isomorphic gradients do have a role in fine tuning skeletal element identities, however (see below), making the boundary model and later accounts of non-isomorphic pattern formation of continuing relevance to limb development.

The gradient system considered in Meinhardt (1983a) is presumed to specify positional identity along the AP axis of the limb bud. In a second paper in this series Meinhardt proposed to unify the generation of PD positional information with that of AP positional information via the same boundary model (Meinhardt, 1983b). This contrasts with the original PI model for this system, which used the idea that there is

an endogenous cellular clock that caused cells in a non-differentiating distal environment (the "progress zone"; Summerbell et al., 1973) to take on more distal fates in proportion to the duration of their residence there. Meinhardt suggested an alternative "bootstrap" model by which proximal differentiating cells signal (by the boundary confrontation mechanism) to the AER, causing it to keep the levels of the morphogen it produces elevated above the values employed to specify the distal-most positional identities of the limb (Meinhardt, 1983b).

Although the described papers do not present detailed mathematical models, they reframed Turing's partial differential equation (PDE)-based chemical reaction-diffusion model in a fashion relevant to developmental systems as "local autoactivation with lateral inhibition" (LALI) mechanisms (reviewed in Meinhardt and Gierer, 2000 and Meinhardt, 2008). Coming before anything was known about the molecular nature of the AER and ZPA signals, Meinhardt insightfully modeled the spatiotemporal dynamics of generic morphogens using the LALI mechanism.

The general form for such Turing-type systems is

$$\frac{\partial C}{\partial t} = D\nabla^2 C + R(C), \tag{6}$$

where C is a vector $(c_1, c_2, ... c_n)$ representing the concentrations of morphogens produced by the cells of the developing organ (e.g., the limb bud) with net rate $R(C)$, and D is a diagonal matrix, the terms of which are the diffusion constants of the morphogens in the tissue. Generalized Turing systems with mixed boundary conditions, inhomogeneous domains and spatially varying diffusivities were studied in Benson et al. (1992), Dillon, (1993), and Dillon et al. (1994) among others. As will be seen below, they have proved useful not only in the analysis of spatiotemporal dynamics of non-isomorphic morphogen patterns, but also provide the underlying modeling framework for most accounts of morphogen patterns isomorphic to the limb skeleton.

16

Othmer and coworkers (Dillon et al., 2003) extended their earlier growth and morphogen patterning model (Dillon and Othmer, 1999) by incorporating newer findings on the Shh signaling pathway, specifically the involvement of the Shh receptor Patched (Ptc) and the associated membrane signal transduction factor, Smoothened (Smo) (Williams et al., 1999; Denef et al., 2000). The problem they addressed was related to experiments in which the spatial profile of Ptc and of Smo-mediated signaling were altered by ectopically introduced Shh. These experiments were difficult to interpret without unsupported assumptions concerning the diffusion rates of different forms of Shh.

In modeling the network of interactions by reaction-diffusion equations in both 1D and in 2D (where the mutual feedback interactions of FGF from the AER and Shh from the ZPA (Niswander et al., 1994) were represented), the authors incorporated new terms for key Shh receptor and mediator proteins, coupled in the 2D case (in addition to terms for FGF) with the Navier-Stokes fluid mechanics equations of their earlier treatment. These models were then used to simulate the effects of ectopic sources of Shh, reproducing experimental results, which in some cases were counterintuitive.

This approach thus exemplified how "reaction" and "diffusion" in biological Turing-type systems could depart from their purely chemical and physical versions, while behaving in a formally similar manner. The signaling network studied involved Shh, the Shh transmembrane receptor Patched (Ptc), and Smoothened (Smo), a transmembrane protein mediating Shh signaling through phosphorylation of the Gli family of transcription factors. Part of the reaction-diffusion system describing the interaction of Shh and Ptc can be described briefly as follows:

[rate of change of Shh] = [diffusion of Shh] – [association of Shh and Ptc] + [disassociation of Shh-Ptc complex] – [degradation of Shh] + [Shh production],

[rate of change of Ptc] = - [association of Shh and Ptc] + [disassociation of Shh-Ptc complex] – [association of Smo and Ptc] + [disassociation and degradation of Smo-Ptc complex] + [Ptc productions by itself and by Smo] – [degradation of Ptc],

[rate of change of Shh-Ptc complex] = [association of Shh and Ptc] - [disassociation and degradation of Shh-Ptc complex],

The system describing interaction of Smo and Ptc is similar. Smo has two forms: the active and inactive forms. Active Smo associates with free Ptc and inactive Smo interacts with the Shh-Ptc complex. By introducing these additional biologically based interactions into their model, the authors were able simulate the different effects of Shh under the assumption that different forms of Shh have the same diffusion constant (Fig. 3). The figure compares simulated and experimental distributions of Shh at successive times after implantation of Shh beads (upper row) or ZPA tissue (lower row). Notably, the simulation reproduce the experimentally observed posterior–anterior *ptc* expression wave followed by restriction of expression near the implant site. Although the assumption of equal diffusion coefficients may not be entirely valid for Shh (see Farshi et al., 2011), the approach of Dillon et al. (2003) was useful in demonstrating the potential impact of network complexity on the physical parameters of the simpler physical systems that serve as paradigms for these developmental models.

A different aspect of the generation of non-isomorphic morphogen patterns in the developing limb was addressed in a reaction-diffusion model by Hirashima et al. (2008). These authors, like Dillon et al. (2003), studied the role of coupled dynamics of positive feedback and feed-forward interaction between FGF expression at the AER and Shh expression at the ZPA, in their case addressing the question of why, given the positive effect FGF on the production of Shh, the sources of the two morphogens remain spatially separated. The model was implemented on a simplified one dimensional domain with AER at the left boundary point and ZPA in the region at a chosen distance from the AER. In accordance with the limb bud's properties, FGF molecules diffuse from the AER and Shh diffuses from the mesenchymal cells, following the usual diffusion equations. To model the feed-forward regulation, the authors postulated a repressor that inhibits *Shh* expression. The coupled dynamics of the repressor and *Shh* expressions were described as follows:

$$\frac{\partial R}{\partial t} = \alpha_R \frac{F^{h_2}}{F^{h_2} + K_2^{h_2}} - \gamma_R R,$$

$$\frac{\partial S_{in}}{\partial t} = \alpha_S \frac{F^{h_1}}{F^{h_1} + K_1^{h_1}} \cdot \frac{K_3^{h_3}}{R^{h_3} + K_3^{h_3}} - (\gamma_{S,in} + \beta_S) S_{in}, \tag{7}$$

The right hand side of the first equation stipulates that the level of repressor R increases with the extracellular FGF concentration F with Hill coefficient h_2. S_{in} denotes the expression level of *Shh* in the mesenchymal cells. $\alpha_R, \alpha_S, \gamma_R,$ and $\gamma_{S,in}$ are parameters for production and degradation of R and *Shh*.

β_S is the rate of transport of Shh to the outside of the cells. $K_1, K_2,$ and K_3 are the dissociation constants, and $h_1, h_2,$ and h_3 are the Hill coefficients.

Drawing on experimental evidence (Lu et al., 2006), the model postulates the *Fgf* expression level in the AER cells, denoted by $F_{in}(t)$, to be stimulated by the extracellular Shh concentration S,

$$\frac{d}{dt} F_{in}(t) = \alpha_F \frac{S^h}{S^h + K^h} - (\gamma + \beta) F_{in}(t), \tag{8}$$

where α_F and γ are the FGF production rate and degradation rate, respectively. β is the rate of active transport of FGF to the extracellular space. K and h are the dissociation constant that gives half-maximal output and the Hill coefficient, respectively, h being assigned different values in different instances of the model. The feedback regulation between the AER and the ZPA makes the distance between them robust to parameter changes, a factor important for their developmental roles. Although several papers have appeared subsequently on the interactions between the AER and ZPA morphogens (e.g., Bastida et al., 2009 and Bénazet et al., 2009, see below), the signaling center spacing model of Hirashima et al., 2008 has yet to be subjected to decisive tests.

Introducing two additional regulatory interactions that influence the expression of the AER and ZPA morphogens FGF and Shh, namely another morphogen, BMP4, and a secreted antagonist of BMP4, Gremlin1 (Grem1), Bénazet et al. (2009) used an ordinary differential equation (ODE) approach (i.e., setting aside for the analysis the contribution of diffusion or other spatial transport of these released factors considered in PDE approaches) to devise a self-regulatory system of interlinked signaling feedback loops. The system has the following form,

$$\frac{dB}{dt} = l - d \cdot G \cdot \left(\frac{B}{B + K_0} \right) - a_B \cdot B$$

$$\frac{dG}{dt} = p_{G1} \left(\frac{B^n}{B^n + K_1^n} \right) + p_{G2} \left(\frac{S^n}{S^n + K_2^n} \right) - a_G \cdot G$$

$$\frac{dS}{dt} = p_S \left(\frac{F^n}{F^n + K_4^n} \right) - a_S \cdot S \tag{9}$$

$$\frac{dF}{dt} = p_F \left(\frac{K_3^n}{K_3^n + B^n} \right) - a_F \cdot F$$

where B, G, S and F represent the concentrations of BMP4, Grem1, Shh and AER sourced FGF (AER-FGF), respectively.

Based on experimental results (for the network connectivity; the kinetic details being largely undetermined), BMP4 is inhibited by Grem1 following Michaelis-Menten kinetics, and d is the maximum inhibition rate per unit of G with K_0 the half saturation. $1/a_B$ is the half-life of the BMP4 protein and BMP4 levels are increased at the constant rate l. Grem1 is positively controlled by both BMP4 and Shh. Hill functions are used to model Grem1, with the maximal velocities p_{G1} and p_{G2}, and the half-maximal induction concentrations corresponding to K_1 and K_2, respectively. The half-life of Grem1 is $1/a_G$. The negative regulation of AER- FGF by BMPs is modeled by a Hill function. p_F is the maximal velocity and K_3 is the half maximal induction concentration. $1/a_F$ is the half-life of FGF protein. The positive

regulation of Shh by AER-FGFs is modeled by a Hill function with maximal velocity p_S, half maximal induction concentration K_4 and a half-life $1/a_S$. n is a common Hill exponent in all equations.

Numerical simulations of this system reproduced the experimental result that BMP4 and Shh activities are mutually antagonistic. Whereas the ODE model did not provide an account of spatial distribution of the morphogens, it enabled simulation of temporal changes in expression of the genes during development. Simulation results, for example, indicated that BMP4, which functions upstream of the genes specifying Grem1 and Shh, first initiates Grem1 expression (at a time corresponding to embryonic day 9), but increasing levels of Grem1 then lowered BMP4 activity rapidly (corresponding to embryonic day 10), which in turn induced the rise of Shh, Grem1, and AER-FGF activities in combination with low and persistent BMP4 activity (seen at embryonic day 11).

The simulations suggested that the interactions considered could explain why intact epithelial-mesenchymal feedback signaling buffers low expression of Shh. Specifically, without an intact Grem1-Bmp4 feedback loop, the loss of one copy of Shh caused a reduction in the number of digits formed, reproducing an experimental result. Other experiments, however, indicate that Shh is not required for the formation of digits, and indeed more digits can form when it is absent than when it is present (Litingtung et al., 2002; Galli et al., 2010).

As with all the other models focused on morphogens non-isomorphic to the skeletal pattern, the underlying assumption of the approach of Bénazet et al. (2009) is that the generated gradients provide positional information for the specification of the skeletal pattern. Experimental verification of this approach would involve demonstration of a genomic "look-up table" or other representation of the mapping between morphogen distributions and cell fates to specify the "interpretation" component of the PI framework (Wolpert, 1969). No such representation has been adduced thus far, and consequently there are no published mathematical or

computational models in this paradigm that simulate the arrangement of limb skeletal elements.

Models involving dynamics of morphogens isomorphic to the skeletal pattern

Wilby and Ede (1975) were the earliest to formulate a mathematical model that produced discrete skeletal elements in a limb-like arrangement. In doing so they explicitly contrasted the modeling strategy of employing a spatially periodic gradient to generate the periodic aspects of the skeleton to the positional information approach, which used one or more monotonic gradients along and required numerous thresholds to encode the interpretation of the gradient(s). These authors rejected, based on its purported instability, a Turing-type reaction-diffusion mechanism for the generation of the quasiperiodic patterns of the skeleton in favor of one based on automata theory, in which cells followed simple rules for differentiation, division, and movement based in part on what their neighbors were signaling. The rules were as follows:

(1) cells are sensitive to their internal concentration of a freely diffusible morphogen M;

(2) at concentrations of M below a lower threshold T1 cells are inactive;

(3) at concentrations of M above T1, cells synthesize M;

(4) at concentrations of M above a higher threshold T2 cells actively destroy M ;

(5) the transformations "inactive to synthetic" and "synthetic to destructive" are irreversible.

These rules are summarized in the following scheme:

$$[\text{Inactive}] \xrightarrow{\text{[M] > T1}} [\text{Synthetic}] \xrightarrow{\text{[M] > T2}} [\text{Destructive}]$$

In the model, diffusion is simulated as a flux F of morphogen concentration M between adjacent cells where $F = d \times ([M]_i - [M]_j)$ per time unit, d being an

arbitrary diffusion constant and $[M]_i$ and $[M]_j$ the concentrations of M in adjacent

cells. The constant d includes the term $1/h^2$ required by Fick's first law, where h is

the distance between cells.

The interactions of synthesis, destruction, and diffusion cause a "trailing" peak of M to stabilize between two areas of destruction and the "leading" peak to initiate a new area of destruction. The end result is a periodic pattern and periodic residual gradient. Linking the initiation of destruction of M with the differentiation of cartilage allows patterning and differentiation to proceed simultaneously but leaves the residual gradient available for further patterning.

Wilby and Ede also presented a modification of their model that simulated partitioning of the pattern along the proximodistal axis by generating a set of limb shapes representing the regions added by growth in each developmental stage, while physically removing the proximal areas once they have been patterned. This "growth increment" version of the model produces a set of small cartilage elements, orientated along the PD axis and showing a distinct posterior-anterior polarity. The model entails an inherent connection between shaping and skeletal patterning of the limb, and indicated that models of its class (i.e., those generating periodicities) could straightforwardly account for normal and abnormal (e.g., mutant) limb development, the results of experimental manipulations such as ZPA grafting and mesoblast reaggregation, and the skeletal forms of extinct tetrapods.

Since the time of Wilby and Ede's model there has been increased acceptance of the applicability of reaction-diffusion-type mechanisms to developmental pattern formation. In particular, increased cell and molecular knowledge has shown (as mentioned above) that "reaction" and "diffusion" functions can be embodied in complex biological processes while still retaining the formal features of the elegant symmetry-breaking schemes of Turing (1952) and Meinhardt and Gierer (2000) (see Kondo and Miura, 2010 for a review). Moreover, the sensitivity of reaction-diffusion systems to variation of parameters and boundary conditions that motivated Wilby and Ede (1975) to seek a more stable alternative becomes less problematic when the

evolutionary dimension is considered. A reaction-diffusion mechanism can provide a range of patterns during the origination of a character such as the limb skeleton, with some forms gradually become stabilized by canalizing selection over time (see Newman et al., 2006). Thus, while the paper of Wilby and Ede (1975) represented a clear conceptual advance in the modeling of limb development, its influence was felt in its emphasis on the limb's inherent periodicity rather than in the relatively ad hoc mechanism it presented.

A few years later, Newman and Frisch (1979) modeled limb development as a quasiperiodic pattern-generating process, but in contrast to Wilby and Ede (1975) they invoked the ability of the reaction-diffusion mechanism to produce chemical standing waves. They reasoned that precartilage condensations could be induced by peaks of a morphogenetic agent, which they identified with the recently characterized ECM protein, fibronectin, found to be elevated in the condensations (Tomasek et al., 1982). Because fibronectin was known to have both soluble and tissue-bound forms they suggested that it acted as both a diffusible morphogen and an aggregating factor. The authors modeled the generation of chemical prepatterns isomorphic to the skeletal elements using the following PDE system (anticipating those later employed by Meinhardt, 1983a,b and Dillon and Othmer, 1999 for the dynamics of non-isomorphic gradients; see above) to describe the production and diffusion of fibronectin in a 3-dimensional tissue:

$$D\nabla^2 c + rc = 0, \tag{10}$$

where c is the molecule's spatially dependent concentration. Although Eq. 10 was not solved in a time-dependent fashion (and indeed the activator-inhibitor circuitry required for the pattern forming instability was not made explicit), it was shown that the system has stationary solutions (for fixed domains) of the form (see also Newman et al.; 1988):

$$X(x)Y(y)Z(z) \tag{11}$$

with

$$X(x) = \sin\frac{m_x \pi x}{l_x} \qquad m_x = 1,2,...$$

$$Y(y) = \sin\frac{m_y \pi y}{l_y} \qquad m_y = 1,2,... \tag{12}$$

$$Z(z) = c_0 e^{\lambda z}$$

where x is the AP axis, y the DV axis and z the PD axis. The x axis is the dimension along which the digits are arrayed. It varies in length in different species, and even between fore and hind limbs of the chicken embryo, where it remains constant during development in the former and expands distally in the latter. The y axis remains of constant length in all developing vertebrate limbs, corresponding to the presence of only single elements in the DV direction at all points along a mature limb.

The z axis varies in length during development as the limb grows out in the PD direction. However, this dimension does not comprise the entire PD length, but only the distal, unpatterned portion of the limb bud within which reaction-diffusion dynamics occurs. This was called the "diffusion chamber" in Newman and Frisch (1979) and variously, the "active" and "LALI" (local autoactivation-lateral inhibition; see above) zones in subsequent versions of the model (see below), and its length, l_z, based on experimental measurements of the unpatterned apical mesenchyme (Summerbell, 1976), actually decreases as the limb grows longer.

A set of stationary solutions of Eq. 10 was provided for different fixed values of l_z during chicken fore limb development, where l_x and l_y are essentially unchanged. The numbers of peaks (defined by the sine wave solutions) in the x and y directions were shown to be constrained by a dispersion relation, subject to a constant, called the "Saunders number," S.

$$\frac{r l_y^2}{\pi^2 D} \equiv S = \frac{m_x^2}{(l_x/l_y)^2} + m_y^2 - \frac{\lambda^2 l_y^2}{\pi^2} \tag{13}$$

In this representation, the distance l_z acts as a control parameter for transitions

in the number of parallel elements (i.e., a single stylopod, two zeugopodal elements, three digits), which increases even though the distance l_y is held constant. Because of the nature of reaction-diffusion systems, as reflected in expression (13), an increase in l_y, which occurs in other types of limbs during development, would lead to a further increase in digit number.

Hentschel et al. (2004) extended the approach of Newman and Frisch (1979) by incorporating a representation of the positively autoregulatory morphogen TGF-β in a system of partial differential equations for skeletal patterning. Since TGF-β is a potent inducer of fibronectin production (reviewed in Newman, 1988), the system also contained an expression for that effect, as well as for the slow diffusion of mesenchymal cells and their positive haptotaxis up gradients of fibronectin, where their density increase is identified with precartilage condensation.

The cells of the developing avian and mouse limbs are regionally differentiated with respect to three functionally different receptors for fibroblast growth factors (reviewed in Ornitz and Marie, 2002), which are skeletally non-isomorphic morphogens produced by both the AER (where FGFs are essential for its activity) and, to a lesser extent, the dorsal and ventral ectoderms (Sun et al., 2002).

Indeed, the four main types of precartilage mesenchymal cells in the developing limb can be defined by their disjoint expression of the three FGF receptors (FGFRs) (Szebenyi et al., 1995). Hentschel et al. (2004) denoted the cells expressing FGFR1, FGFR2 and FGFR3, respectively, by R_1, $R_2 + R_2'$ and R_3. (See Filion and Popel, 2004, for a reaction-diffusion scheme also employing an FGF and its receptors). The cells designated as R_2' are a subset of those bearing FGFR2, but at a slightly later stage, when they have begun to produce fibronectin. In their model the authors presented equations for the spatially and temporarily varying densities and dynamics of interconversion of these different cell types. Based on evidence that the cells that initially bear FGFR2 are the source of a laterally acting inhibitor of precartilage condensation (Moftah et al., 2002), the authors also incorporated an equation for the

dynamics of this uncharacterized inhibitor. The result was an eight-equation PDE system representing the "core mechanism" of limb skeletal pattern formation:

$$\partial c / \partial t = D\nabla^2 c - kc + J(x,t)$$

$$\partial c_a / \partial t = D_a \nabla^2 c_a - k_a c_i c_a + J_a^1 R_1 + J_a(c_a) R_2$$

$$\partial c_i / \partial t = D_i \nabla^2 c_i - k_a c_i c_a + J_i(c_a) R_2$$

$$\partial R_1 / \partial t = D_{cell} \nabla^2 R_1 - \chi \nabla \cdot (R_1 \nabla \rho) + r R_1 (R_{eq} - R) + k_{21} R_2 - k_{12}(c, c_a) R_1$$

$$\partial R_2 / \partial t = D_{cell} \nabla^2 R_2 - \chi \nabla \cdot (R_2 \nabla \rho) + r R_2 (R_{eq} - R) + k_{12} R_1 - k_{21} R_2 - k_{22} R_2 \quad (14)$$

$$\partial R_2' / \partial t = D_{cell} \nabla^2 R_2' - \chi \nabla \cdot (R_2' \nabla \rho) + r R_2' (R_{eq} - R) + k_{22} R_2 - k_{23} R_2'$$

$$\partial R_3 / \partial t = r_3 R_3 (R_{eq} - R_3) + k_{23} R_2'$$

$$\partial \rho / \partial t = k_b (R_1 + R_2) + k'_b R_2' - k_c \rho$$

In this scheme, c, c_a, c_i and ρ denote, respectively, the spatially and temporarily varying concentrations of FGFs (produced by the ectoderm), TGF-β (produced throughout the mesenchyme), a diffusible inhibitor of chondrogenesis produced by R_2 cells, and fibronectin, produced by R_2' cells. In addition, As noted, R_1, R_2, R_2' and R_3 are densities of the different kinds of cells, but since FGFR3 is only expressed by differentiated cartilage cells, which are immobile, $R = R_1 + R_2 + R_2'$ is the density of the mobile cells of the developing limb. A schematic representation of the model of Hentschel et al. (2004) is shown in Fig. 4.

Hentschel and coworkers presented simulations based on a 2D version of their model using biologically motivated simplifications of the dynamics. The model remained a purely continuum one, however, with distributions of the various cell types appearing as density functions. Moreover, like the model of Newman and Frisch (1979) on which it was based, the simulations were confined to obtaining stationary solutions of the morphogen and cell distributions in domains of fixed size representing the

unpatterned portion of the limb bud at successive stages of development.

These limitations have been overcome by adopting a hybrid discrete-continuous computational approach to simulating the interaction of cells and morphogens in the developing limb. Izaguirre et al. (2004) and Cickovski et al. (2005) introduced a multi-model computational framework integrating continuous equations and discrete models. The framework consists of three main parts. The Cellular Potts model (CPM; Graner and Glazier, 1992; Glazier and Graner, 1993), describing cell and ECM behavior, a reaction-diffusion PDE system describing the formation of skeletal prepatterns in a growing domain, and an ODE model comprising gene regulatory networks (GRNs), the multistable stationary states of which represent differentiated cell types.

The CPM, the discrete, agent-based component of the framework also referred to as the Glazier-Graner-Hogeweg model (Scianna and Preziosi, 2013), performs energy minimization calculations on generalized cells, which can be actual cells or adjoining regions of the ECM, represented in the model as simply-connected domains of pixels. A *contact energy* $E_{Contact}$, defined between pairs of generalized cells, describes the net adhesion/repulsion at their interface. An area (2D) or volume (3D) energy, E_{Volume}, penalizes the deviation of a cell from its target value in the minimization calculation. The effective energy E is a function of $E_{Contact}$ and E_{Volume}, as well as cell differentiation and division, and responses to external chemical stimuli. E contains true energies (e.g., cell-cell adhesion) and terms that mimic energies (e.g., chemical fields modeling the cell's response to chemotactic and haptotactic gradients):

$$E = E_{Contact} + E_{Volume} + E_{Chemical}, \qquad (15)$$

and is minimized in the CPM in the dissipative limit using Metropolis Monte Carlo dynamics (Metropolis et al., 1953).

Simulations of limb skeletal development were performed on a 2D plane by

28

Izaguirre et al. (2004) using as the reaction-diffusion component the well-studied but ad hoc Schnakenberg 2-equation PDE system (Murray, 2002), a simple two-state transition function between nonaggregating and aggregating cells, responsive to threshold values of the presumed activating morphogen and, as in Newman and Frisch (1979), a succession of fixed spatial domains. Cickovski et al. (2005) improved on this by using a simplified version of the biologically motivated PDE system of Hentschel et al. (2004), chemical fields and response functions to represent both chemotaxis and haptotaxis of cells to elevated levels of fibronectin (produced in response to elevated levels of activating morphogen (TGF-β), as specified in a more elaborate cell-type transition map than that of Izaguirre et al., 2004), and the dynamical establishment of the morphogenetically active zone by a balance of cell multiplication and the inhibitory effect of a distally sourced inhibitory gradient (FGF) representing the AER. All of this was computed on a 3D CPM grid (i.e., with the third, dorsoventral, dimension made explicit), where it produced an increasing number of parallel elements in a proximodistal sequence, as in the living embryo (Cickovski et al., 2005).

In contrast to Cickovski et al. (2005), who modeled only "noncondensing" and "condensing" cells, Chaturvedi et al. (2005) employed a cell-state transition map using the full range of cell types in the model of Hentschel et al. (2004), R_1, R_2, R_2' and R_3. Another difference between these two studies was that whereas Cickovski et al. (2005) permitted the width of the active zone to change in an emergent fashion by incorporating the movement of proliferating cells away from the high point of FGF at the AER, Chaturvedi et al. (2005) changed the aspect ratio of the active zone by programmatic alteration of the values of the morphogen diffusion coefficients. Successive stationary patterns were then computed as in Newman and Frisch (1979).

Cickovski et al. (2005) and Chaturvedi et al. (2005) thus each incorporated realistic aspects of the biology into their respective models, but in the absence of relevant experimental data, and in consideration of necessary simplifications for feasible 3D simulations, some of the choices made were arbitrary and mutually

29

exclusive. Examples of these studies' results are shown in Fig. 5. Panel (A) shows a simulation from Chaturvedi et al (2005) of the active zone TGF-β profile over successive times (vertical axis); panel (B) shows three simulations of the cell density profiles (condensed cells shown in gray).for successive times during limb development, from Cickovski et al. (2005),

While the model of Hentschel et al. (2004) was based on available cell biological and molecular genetic circuitry of the developing limb, the finding of arithmetically increasing numbers of skeletal elements seen in these two computational implementations is mechanistically "underdetermined." For example, similar patterns and pattern transitions were seen in a model based on chemotaxis, a mechanism not known at the time to be involved in mesenchymal condensation (Myerscough et al., 1998; however, see Mammoto et al., 2011 for evidence that chemotaxis operates during tooth bud formation).

In both Cickovski et al. (2005) and Chaturvedi et al. (2005) the elaborate "reactor-diffusion" dynamics of the full model of Hentschel et al. (2004) were reduced to a simpler form in different computationally convenient, but biologically and mathematically informal, ways. A preferable strategy for evaluating the validity of the model, however, is to perform the reduction in a mathematically rigorous fashion, using explicit biological idealizations. In this way, any deficiencies in its predictions can be traced to known assumptions. Alber et al. (2004), in one of the few purely analytical mathematical results in this field, studied the conditions under which the full system (Eqs. 14) was guaranteed to have smooth solutions that exist globally in time. It was also shown by introducing arbitrarily small diffusion of fibronectin, that the number of conditions necessary for the global existence of smooth solutions can be significantly reduced. By itself, however, this analysis was not sufficient to characterize the asymptotics of the long-time solutions determining the system's final patterns, or to identify the parameter set within which biologically relevant simulations could be performed.

The main obstacle to applying the standard parabolic equations approach was the presence of the terms proportional to $\nabla^2 \rho$ in the equations for the moving cells.

The change of variables introduced in (Friedman and Tello 2002) was used and the contraction mapping theorem (Fontelos, Friedman and Hu 2002) was applied for proving the existence of a solution for $t \in (0,T)$, with $T > 0$ sufficiently small.

The full system in fact is "morphodynamic," in the sense that cell movement by haptotaxis occurs simultaneously with the generation of morphogen patterns and cell differentiation (Salazar-Ciudad et al. 2003). Under the alternative but also biologically plausible "morphostatic" assumption (Salazar et al., 2003), however, which postulates that the distribution of the key morphogens and the induced cell differentiation pattern relaxes faster than the evolution of the overall cell density, it became possible to analytically extract from the full eight-equation system a simplified two-equation subsystem governing the interaction of two of the key morphogens: the activator and an activator-dependent inhibitor of precartilage condensation formation (Alber et al., 2008). The reduced system has the form:

$$\begin{cases} \dfrac{\partial c_a}{\partial t} = D_a \nabla^2 c_a + U(c_a) - k_a c_a c_i, \\ \dfrac{\partial c_i}{\partial t} = D_i \nabla^2 c_i + V(c_a) - k_a c_a c_i, \end{cases} \qquad (16)$$

The above equations incorporate diffusion and decay of morphogens, along with the terms $U(c_a)$ and $V(c_a)$, which describe the production of activator and inhibitor by the cells. These production rates depend on the concentration c_a of the activator itself.

The exact forms of these production terms $U(c_a)$ and $V(c_a)$ are as follows

$$\begin{aligned} U(c_a) &= [J_a^1 + J_a(c_a)\beta(c_a)]R_{eq}, \\ V(c_a) &= J_i(c_a)\beta(c_a)R_{eq}, \end{aligned} \qquad (17)$$

where

$$J_a(c_a) = J_{a\max}(c_a/s)^n /[1+(c_a/s)^n], \qquad J_i(c_a) = J_{i\max}(c_a/\delta)^q /[1+(c_a/\delta)^q], \qquad \text{and}$$

$\beta(c_a) = \beta_1 c_a /(\beta_2 + c_a)$. J_a^1 and the Michaelis-Menten type functions $J_a(c_a)$, $\beta(c_a)$, and $J_i(c_a)$ are the rates at which the various cell types release TGF-β and the inhibitor, and these cells have a same equilibrium density R_{eq} (see Hentschel et al., 2004). The

31

system is subject to no-flux boundary conditions and zero initial concentrations for c_a and c_i.

The reaction kinetic parameters λ and δ appear in the production rates of activator and inhibitor morphogens and their values dramatically affect the generated patterns. In the model λ describes the feedback strength of the activator morphogen, and δ denotes the activator morphogen concentration which separates the linear response phase from the saturation response phase (Alber et al., 2008). Biologically, these parameters are proposed to be related to the distributions of Hox gene products in the apical zone at the different phases of limb development (Nelson et al., 1996), with the rationale that Hox proteins are transcription factors that regulate the levels of developmentally important signals such as the activating and inhibitory morphogens (Svingen et al., 2006).

The full model of Hentschel et al. (2004) contains expressions for activating and inhibitory morphogens and their interactions with cells (which are reduced to Eqs. 16-17 under the morphostatic assumption). Also, by the evolution of the distribution of the AER morphogen FGF (concentration denoted by c) and the dependency of the mass of R_1 precartilage mesenchymal cells on this factor, the resulting patterns are caused to develop in a progressive spatiotemporal direction, as in the actual limb. In addition to this polarity of growth, and the transitions in element number induced by the AER-regulated change in aspect ratio of the LALI zone, as with any reaction-diffusion-type system the shape and boundary values of the relevant domain will effect the details of the patterns generated. Two aspects of limb development that have generally been subjects of separate mathematical modeling efforts – limb bud shaping and skeletogenesis (see above) – are thus interrelated and should eventually be incorporated into unified models.

Recently, a moving grid discontinuous Galerkin (DG) finite element method was introduced for modeling skeletal pattern formation in the vertebrate limb (Zhu et al., 2009a,b). The DG method provides means for converting an ordinary or partial differential equation system into a problem represented by a system of algebraic

equations in a more restricted space than that of the original system. It employs "independent" polynomials on every element to approximate the system's behavior in the restricted space and provides more flexibility than the continuous Galerkin finite element method. This method enables numerical solutions of reaction-diffusion systems on deforming and moving grids in domains with complicated geometries and moving boundaries. (See Madzvamuse et al., 2005 for an allied approach.) To approximate the irregular geometries of limb buds, the cubic spline interpolation technique (de Boor 2001) was used in (Zhu et al., 2009a,b). This method approximates the curved boundary of a limb bud by piece-wise cubic polynomials and maintains global smoothness of the obtained spline curve.

Based on the earlier-described proposed mechanism spatiotemporal skeletal pattern formation (Hentschel et al., 2004; Newman and Bhat, 2007), reaction and diffusion of morphogens occurs in the LALI zone, the activator morphogen induces pattern elements in the active zone (the proximal portion of the LALI zone), and these elements become consolidated in the frozen zone. As the frozen zone grows, the LALI zone's width shrinks and its shape deforms. The LALI zone, which denoted by $\Omega(t)$, resides at the distal tip of the developing limb. Because the morphogen system denoted by Eqs. 16-17 is defined on a moving domain, $\Omega(t)$, all spatial variables (x, y) are functions of time, t. By the Reynolds transport theorem (Kundu, 1990), the system (16) on a moving domain will be

$$\begin{cases} \dfrac{\mathscr{D} c_a}{\mathscr{D} t} + c_a \nabla \cdot \vec{a} = D_a \nabla^2 c_a + U(c_a) - k_a c_a c_i, \\ \dfrac{\mathscr{D} c_i}{\mathscr{D} t} + c_i \nabla \cdot \vec{a} = D_i \nabla^2 c_i + V(c_a) - k_a c_a c_i, \end{cases} \tag{18}$$

where $\dfrac{\mathscr{D}}{\mathscr{D} t}$ (= $\dfrac{\partial}{\partial t} + \vec{a} \cdot \nabla$) is the material derivative, and $\vec{a}(x(t), y(t), t) = \begin{pmatrix} dx(t)/dt \\ dy(t)/dt \end{pmatrix}$

is the velocity of a spatial point $(x(t), y(t))$ in the moving LALI zone $\Omega(t)$.

The moving velocity $\vec{a}(x(t), y(t), t)$ of the LALI zone is determined by the aspect ratio of the LALI zone at different stages, which determines the number of parallel elements in the reaction-diffusion model (Newman and Frisch, 1979; Hentschel et al.,

2004; Zhu et al., 2009b). Since the natural shape of a developing limb is nonstandard, the discontinuous Galerkin finite element method (Zhu et al., 2009a; Zhu et al., 2009b) was used to describe the complicated geometries and solve the system (3) on the moving domain $\Omega(t)$ numerically.

The core chondrogenic mechanism of the developing limb in the presence of an FGF gradient was simulated using the computational model described above, which permits simulation of LALI systems in domains of varying size and shape. The model predicts the normal proximodistal pattern of skeletogenesis as well as distal truncations resulting from AER removal (Saunders, 1948) (Fig. 6), and a variety of limb bud-deforming mutations and other conditions (Zhu, et al., 2009b; Zhu, et al., 2010).

A biologically valid model of limb skeletogenesis should not only be capable of simulating the limbs of present-day animals, but also provide a mechanistic rationale for the appearance of a limb-type skeletal pattern at the fin-limb transition at the origin of the tetrapods (Hinchliffe et al., 2002). Zhu et al. (2010) thus sought to test whether their model, with adjusted kinetic parameters and limb bud contours, but conserved regulatory network topology and AP FGF gradient dynamics and emergent zone assignments, could reproduce the features of fossil limb skeletons, including some from extinct fish-like ancestors and ichthyosaurs, i.e., swimming dinosaurs. Since the embryology is unknown for the extinct species, the authors designed a range of hypothetical developmental scenarios. The simulation end-points shown alongside drawings of fossil limbs in Fig. 7 indicate that their model exhibits sufficient flexibility to reproduce the general features of limb skeletons of a variety of pre-tetrapods (such as the lobe-finned fish *Tiktaalik*; Shubin et al., 2006) with limb-like appendages.

Relevance of morphodynamic effects

Computational tractability of the LALI-type models described above have typically involved making the morphostatic assumption that pattern formation is mechanistically separated from cell movement. A more authentic treatment, however, would be morphodynamic, as in Hentschel et al. (2004), where the cellular "reactors"

that generate the morphogens and extracellular molecules which mediate cell condensation undergo rearrangement simultaneously with (and in reaction to) their production of these agents. For small, local cell translocations the full morphodynamic process may yield the same results as the idealized morphostatic one, but as seen in the work of Salazar-Ciudad and Jernvall on the positioning of tooth cusps, morphodynamic effects can have dramatic consequences for developmental and evolutionary change (Salazar-Ciudad and Jernvall, 2005; 2010).

After the appearance of the reaction-diffusion model of Newman and Frisch (1979), Oster and coworkers adapted the LALI formalism to a mechanical interpretation in which pattern formation and morphogenesis (i.e., mesenchymal condensation) were reflections of a single process, the contraction of the intercellular matrix by mechanical stresses exerted locally by the cells themselves. A patterned (as opposed to global) contraction was effected in their model by invoking elastic attenuation by ECM away from the centers of contraction. They analogized their mechanism to a reaction-diffusion process, in which contraction was proposed to play the role of a short-range activator, and elastic attenuation that of a long-range inhibitor (Oster et al, 1983).

Although this model thus featured a pattern-forming mechanism of which cell movement was an intrinsic component, several observations tended to disconfirm it. One was the recognition that in contrast to fibrous collagen ECMs (e.g., Stopak and Harris, 1982), the amorphous hyaluronan-glycoprotein matrix of the limb mesenchyme cannot sustain the cell traction-dependent deformations required by the model of Oster et al. (1983). Moreover, in vivo evidence indicated that the limb skeletal pattern was set well before condensation of the skeletal primordia occurred (Wolpert and Hornbruch, 1990).

Recent work, however, has revived consideration of patterning mechanisms that depend on cell movement. A study of the role of the multifunctional galectin proteins in chick limb development (Bhat et al., 2011, discussed in Section 2, above), identified an early stage of skeletal development in which "protocondensations" are mediated by CG-1A, a galectin that acts as both a morphogen and a matricellular adhesion protein.

The regulatory network formed by CG-1A and its modulatory partner CG-8 constitute a LALI-type system with distinct morphodynamic properties. In particular, a PDE model adhering closely to the cell-molecular interactions identified in Bhat et al. (2011) readily produces periodically patterned skeletal primordia only when a cell flux term is included in the system of equations (T. Glimm, personal communication).

Heuristic models relating to the LALI framework for skeletogenesis

A series of special-purpose models have been presented over the past decade that while not attempting to represent the development of the limb skeleton in anything like its multiscale complexity, are instead directed toward testing the sufficiency of the LALI framework for skeletal pattern formation. In some cases the simplification was in the system modeled, allowing for simulation of detailed cellular behaviors and quantitative comparisons with broad ranges of experimental variability. On other cases highly simplified reaction-diffusion models have been used to assess their generic capacity to account for some puzzling genetic variations of the limb skeleton.

In the category of simpler experimental settings, Miura and Shiota (2000b) produced planar "micromass" cultures of limb bud mesenchyme. In this in vitro system, patterns of precartilage condensations form and cartilage nodules differentiate with a time-course and on a spatial scale similar to that in the embryo (Leonard et al., 1991; Downie et al., 1994). Miura and Shiota grew their cultures within collagen or agarose gels of different densities and found that the condensation pattern became less coarse with increased gel density. Using a computational model that implemented the assumptions of a reaction-diffusion mechanism, a cell sorting mechanism based on differential adhesion, and the cell traction model of Oster et al. (1983), they determined that the experimental data were consistent with the first two mechanisms, but not the third.

Later, a multiscale, stochastic, discrete approach was used to model chondrogenic pattern formation in the micromass system (Kiskowski et al., 2004; Christley et al., 2007). Both models were calibrated using experimentally determined or biologically plausible data on rates of cell and activator and inhibitor morphogen

movement. In Kiskowski et al. (2004), cells and the molecules they produce (with formal properties of a positively autoregulatory activator, an inhibitor, and fibronectin-type ECM) were modeled as mobile single-pixel agents that implemented rules concerning production and response to the molecules (also represented as single pixels). The importance of lateral inhibition for achieving authentic condensation pattern statistics was exemplified in this study: when the strength of this branch of the core cell-molecular regulatory was attenuated the regularity of the pattern was correspondingly degraded.

In Christley et al. (2007), cell and molecular dynamics were simulated on distinct spatial and temporal scales with cells represented as spatially extended multipixel objects that could change their shape. Simulation results indicated that cells can form condensation patterns by undergoing small displacements of less than a cell diameter, packing more closely at sites of ECM accumulation by changing their shapes, while maintaining a relatively uniform cell density across the entire spatial domain. In both Kiskowski et al., 2004 and Christley et al., 2007 regions of parameter were identified in which both condensation size and spacing fell within the envelope of experimentally determined values.

The simulations in Christley et al. (2007) disclosed two distinct dynamical regimes for pattern self-organization involving transient or stationary inductive patterns of morphogens. In the transient regime patterns of activator and inhibitor morphogen concentrations appeared for a brief period of time after which the patterns degraded. In the stationary regime a spatial pattern of morphogen concentrations formed that remained stable over time. Sensitivity analysis of key parameters indicated robustness in pattern formation behavior with some realistic variation in the morphological outcomes. For example, formation of both spots and stripes of precartilage condensation (as seen in the cultures) could be produced by the model under slightly different parameter choices.

As noted above (Section 2), FGF family morphogens not only suppress pattern formation distally in the intact limb, but also act as modulators of the presumed reaction-diffusion network by, for example, eliciting a lateral inhibitor of condensation

in cells that bear the FGFR2 receptor (Moftah et al., 2002). Drawing on observations from the micromass culture system, Miura and Maini (2004) investigated the effect of FGF4 on the speed of the emergence of the condensation pattern. They showed analytically, and confirmed by numerical simulations, that the rate of pattern emergence can change abruptly with small parameter changes if the system is governed by a diffusion-driven instability. Representing the system in terms of the Gierer-Meinhardt reaction-diffusion model indicated that a change in a single parameter can in principle explain two experimentally determined effects of FGF on limb mesenchyme cells: reinforcement of lateral inhibition and earlier appearance of pattern.

In the category of highly schematic models of features of the intact limb, Miura et al. (2006) studied the digital pattern in *Doublefoot* (*Dbf*) mutant mice, which have supernumerary digits due to overexpansion of the limb bud. In this mouse strain thin digits exist in the proximal part of the hand or foot, which sometimes become normal abruptly in the distal part, an effect difficult to explain in the positional information (PI) framework. By numerical simulation of the simplest possible Turing-type reaction–diffusion model on a growing domain, they found that exactly the same "mixed-mode" patterning behavior was reproduced. They then analytically related this pattern outcome to the saturation of activator kinetics in the model. Their analysis led to the prediction that the inverse of the typical *Dbf* pattern, i.e., thin proximodistal channels within thick digits, was also consistent with the reaction-diffusion mechanism, and they in fact found an example of this among their mutant embryos.

In another example of the application of simplified models, Glimm et al. (2012), sought to understand the patterning effects of modulating the reaction parameters of a Turing-type system by a graded modifier orthogonal to the standing wave solution. This, of course, potentially represents the effect of Shh emanating from the ZPA under the assumption that the digits are patterned by a reaction-diffusion process. Using a generalized representation of a reaction-diffusion system as well as the specific case of the Schnakenberg equations (Murray, 2002), the authors present both analytical and numerical results demonstrating the subtle and often counterintuitive effects of

modulatory gradients on Turing patterns (Fig. 8). Examples of anomalies in limb development such as the loss of a middle finger in mouse embryos that were genetically modified such that a shallower Shh gradient was present in the limb buds (Harfe et al., 2004), the formation of an ectopic digit posterior to mouse digit V when the Hedgehog signaling pathway was abrogated in the limb ectoderm (Bouldin et al., 2010), and the fusion of digits seen in human Triphalangeal thumb-polysyndactyly syndrome, in which a limb-specific enhancer of Shh expression is duplicated (Sun et al. 2008; Wieczorek et al., 2010; Klopocki et al. 2008), all of which are difficult to reconcile with the PI model, prove to be consistent with the results of the analysis gradient-Turing mechanism interactions.

4. Conclusions and Discussion

In this review we have described a variety of mathematical modeling approaches to the study of vertebrate limb development. These include models focusing on outgrowth and shaping of the limb bud, models concerned with the establishment of morphogen gradients such as FGF and Shh that are non-isomorphic to the skeletal pattern, several of which control outgrowth and shaping and some of which modulate the details of the skeletal elements, and models concerned with the generation and arrangement of the skeleton itself.

The relevant biological mechanisms operate at a variety of temporal and spatial scales and involve cell-cell signaling, gene expression regulation, including cell-type transitions, cell movement, and viscoelastic behavior of both epithelial and mesenchymal tissues. Modeling this broad range of biological processes has required a correspondingly rich set of mathematical techniques, among which are continuum approaches, immersed boundary and finite element methods, discrete methods such as cellular automata and stochastic systems, and partial differential equations. The limb thus constitutes one of the most comprehensive systems for experiment-based modeling in the field of developmental biology.

In addition to the insights mathematical modeling has made to understanding

vertebrate limb development, the problems raised by this system have also stimulated the generation of new modeling strategies. Specifically, the limb problem motivated what may have been the first biological application of Turing-type reaction-diffusion system in which experimental data on cell and molecular properties and tissue dimensions were taken into consideration, as well as sensitivity of pattern properties to the changing size of a small (i.e., wavelength-comparable) domain (Newman and Frisch, 1979). CompuCell and CompuCell3D (http://www.compucell3d.org/), versatile and widely used multiscale simulation environments incorporating the Cellular Potts model (CPM) (Glazier and Graner, 1993, Scianna and Preziosi, 2013) for cell and ECM behavior, along with reaction-diffusion equations for morphogen dynamics and cell transition dynamics via ordinary differential equations, were first tested on the limb (Izaguirre et al., 2004; Cickovski et al., 2005; Chaturvedi et al., 2005). Such multiscale approaches, coupling discrete stochastic and deterministic continuous submodels, are increasingly seen as crucial to new hypothesis generation based on large data sets, and have been invaluable in other areas of developmental biology (Schnell et al., 2008), and in cell biological and multicellular problems (Chauvière and Preziosi, 2010; Anderson et al., 2007; Asthagiri and Arkin, 2012) including blood clot formation (Xu et al., 2012) and cancer (Deisboeck and Stamatakos, 2010).

The problem of limb development, furthermore, motivated what may be the first detailed mathematical investigation of the analytical properties of an experimentally based multidimensional set of coupled reaction-diffusion equations for a developmental process (Alber et al., 2004), and the formulation of a new discontinuous Galerkin moving grid approach grids for the finite element modeling of reaction-diffusion systems (Zhu et al., 2009a).

Several unresolved questions concerning limb morphogenesis and pattern formation continue to be under active investigation and are likely to yield to combined experimental, mathematical and computational approaches in the coming years. These include the relation of Hox gene activity to the core reaction-diffusion mechanism of skeletogenesis (J. Sharpe, personal communication), the development of a realistic morphodynamic (*sensu* Salazar-Ciudad et al., 2003) model incorporating

cell flux to represent the newly identified dynamics of early "protocondensation" formation in the embryonic limb (Bhat et al., 2011) (T. Glimm, personal communication), and the reconciliation of the variously proposed oriented cell and tissue rearrangements that drive limb bud outgrowth (Hopyan et al., 2011).

The model by Boehm et al. (2010) has taken the use of quantitative measurements to inform models and establish causal mechanisms for the generation of limb bud outgrowth and shape to an unprecedented level. Although the complexity of the core skeletal patterning process and the abundance of molecular components involved in the molding of individual skeletal elements will probably preclude analysis of these mechanisms at a similar level of resolution in the near term, its possibility is a motivating ideal. In the meantime, phenomenological and heuristic models, and those that simulate simplified experimental systems such as pattern formation in the micromass cell culture system will continue to contribute to the overall picture. The success of multidisciplinary, multiscale strategies over the last several decades in building a coherent understanding of limb development provides encouragement regarding the next phase of this research.

References

M. Alber, H.G.E. Hentschel, B. Kazmierczak, S. A. Newman. Existence of solutions to a new model of biological pattern formation. J. Math. Anal. Appl., 308 (2004), 175--194.

M. Alber, T. Glimm, H.G.E. Hentschel, B. Kazmierczak, Y.-T. Zhang, J. Zhu, S.A. Newman. The morphostatic limit for a model of skeletal pattern formation in the vertebrate limb. Bulletin of Mathematical Biology, 70 (2008), 460--483.

A.R.A. Anderson, M.A.J. Chaplain, and K.A. Rejniak, editors, *Single-Cell-Based Models in Biology and Medicine*, 349 pages, Birkhäuser Verlag, Basel (2007).

A. R. Asthagiri, A. Arkin, editors, *Computational Methods in Cell Biology*, Volume 110, Editors: 370 pages (2012).

M. F. Bastida, R. Sheth and M. A. Ros, A BMP-Shh negative-feedback loop restricts Shh expression during limb development. Development, 136 (2009), 3779-3789.

J.-D. Bénazet, M. Bischofberger, E. Tiecke, A. Gonçalves, J.F. Martin, A. Zuniga, F. Naef, R. Zeller, A self-regulatory system of interlinked signaling feedback loops controls mouse limb patterning, Science, 323 (2009), 1050-1053.

D.L. Benson, J.A. Sherratt and P.K. Maini, Diffusion driven instability in an inhomogeneous domain, Bull. Math. Biol., 55 (1992), 365-384.

R. Bhat, K.M. Lerea, H. Peng, H. Kaltner, H.-J. Gabius and S.A. Newman. A regulatory network of two galectins mediates the earliest steps of avian limb skeletal morphogenesis. BMC Dev Biol., 11 (2011), 6.

B. Boehm, H. Westerberg, G. Lesnicar-Pucko, S. Raja, M. Rautschka, J. Cotterell, J. Swoger and James Sharpe, The role of spatially controlled cell proliferation in limb bud morphogenesis, PLoS Biol., 8 (2010), e1000420.

V.G. Borkhvardt. The growth and form development of the limb buds in vertebrate animals. Ontogenez., 31(2000), 192-200.

C. M. Bouldin, A. Gritli-Linde, S. Ahn and B. D. Harfe, Shh pathway activation is present and required within the vertebrate limb bud apical ectodermal ridge for normal autopod patterning. Proc Natl Acad Sci U S A, 107 (2010), 5489-5494.

J. Bowen, J.R. Hinchliffe, T.J. Horder and A.M. Reeve. The fate map of the chick forelimb-bud and its bearing on hypothesized developmental control mechanisms. Anat Embryol., 179(1989), 269-83.

R. Chaturvedi, C. Huang, B. Kazmierczak, T. Schneider, J.A Izaguirre, T. Glimm, H.G.E. Hentschel, J.A. Glazier, S.A. Newman, and M.S Alber, On multiscale approaches to three-dimensional modelling of morphogenesis, J R Soc Interface., 2(2005), 237–253.

A. Chauvière, L. Preziosi (Eds.), Cell Mechanics: From Single Scale-Based Models to Multiscale Modeling (Chapman & Hall/CRC Mathematical & Computational Biology), 482 pages (2010).

Y. Cheng and C.-W. Shu, A discontinuous Galerkin finite element method for time dependent partial differential equations with higher order derivatives. Mathematics of Computation, 77 (2008), 699 -- 730.

S. Christley, M. S. Alber and S. A. Newman, Patterns of mesenchymal condensation in a multiscale, discrete stochastic model. PLoS Comput Biol, 3 (2007), (e76) 0743-0753.

T.M. Cickovski, H. Chengbang, R. Chaturvedi, T. Glimm, H.G.E. Hentschel, M.S. Alber, J.A. Glazier, S.A. Newman, J. Izaguirre, A framework for three-dimensional simulation of morphogenesis, Computational Biology and Bioinformatics., 2(2005), 273 – 288.

B. Cockburn and C.-W. Shu. TVB Runge-Kutta local projection discontinuous Galerkin finite element method for conservation laws II: general framework. Mathematics of Computation, 52(1989), 411-435.

B. Cockburn and C.-W. Shu. Runge-Kutta discontinuous Galerkin method for convection-dominated problems. Journal of Scientific Computing, 16 (2001), 173-261.

E.J. Crampin, W.W. Hackborn and P.K. Maini, Pattern formation in reaction-diffusion models with nonuniform domain growth, Bulletin of Mathematical Biology, 64 (2002a), 747-769.

E.J. Crampin, E. A. Gaffney, P. K. Maini, Mode-doubling and tripling in reaction-diffusion patterns on growing domains: A piecewise linear model, J. Math. Biol., 44(2002b), 107–128.

B. J. Damon, N. V. Mezentseva, J. S. Kumaratilake, G. Forgacs, and S.A. Newman, Limb bud and flank mesoderm have distinct "physical phenotypes" that may contribute to limb budding. Dev Biol, 321(2008), 319-30.

C. de Boor, A practical guide to splines. (2001). New York: Springer.

T. S. Deisboeck, G. Stamatakos, editors, *Multiscale Cancer Modeling*, Chapman & Hall/CRC Mathematical & Computational Biology, CRC Press - 484 Pages (2010).

N. Denef, D. Neubüser, L. Perez, S.M. Cohen. Hedgehog induces opposite changes in turnover and subcellular localization of patched and smoothened. Cell, 102(2000), 521-31.

R. Dillon and H.G. Othmer. A mathematical model for outgrowth and spatial patterning of the vertebrate limb bud. J. Theor. Biol., 197(1999), 295 – 330.

R. Dillon, Mathematical modeling of vertebrate limb development, in Mathematical models for biological pattern formation (edited by P.K. Maini and H.G. Othmer). (2001). Springer-Verlag, New York, Inc.

R. Dillon, A mathematical model of vertebrate limb development with modulated reaction and diffusion, PhD thesis, University of Utah, (1993).

R. Dillon, P.K. Maini and H.G. Othmer, Pattern formation in generalized Turing systems I. Steady-state patterns in systems with mixed boundary conditions, J. Math. Biol., 32(1994), 345-393.

R. Dillon, C. Gadgil and H.G. Othmer, Short- and long-range effects of sonic hedgehog in limb development, Proc. Nat. Acad. Sci., 100(2003), 10152-10157.

S. A. Downie and S. A. Newman, Morphogenetic differences between fore and hind limb precartilage mesenchyme: relation to mechanisms of skeletal pattern

formation. Dev Biol, 162(1994), 195-208.

P. Farshi, S. Ohlig, U. Pickhinke, S. Höing, K. Jochmann, R. Lawrence, R. Dreier, T. Dierker, K. Grobe, Dual roles of the Cardin-Weintraub motif in multimeric Sonic hedgehog. J Biol Chem., 286(2011), 23608-19.

M.A. Fontelos, A. Friedman, B. Hu, Mathematical analysis of a model for the initiation of angiogenesis, SIAM J. Math. Anal. 33 (2002) 1330–1355.

A. Friedman, J.I. Tello, Stability of solutions of chemotaxis equations in reinforced random walks, J. Math. Anal. Appl. 272 (2002) 138–163.

R. Fujimaki, Y. Toyama, N. Hozumi, K. Tezuka. Involvement of Notch signaling in initiation of prechondrogenic condensation and nodule formation in limb bud micromass cultures. J Bone Miner Metab., 24(2006), 191-8.

D. A. Garzón-Alvarado, J. M. García-Aznar and M. Doblaré, A reaction–diffusion model for long bones growth, Biomechan. Modeling Mechanobiol, 8(2009), 381-395.

J.A. Glazier, F. Graner. A simulation of the differential adhesion driven rearrangement of biological cells. Physical Review Part E., 47(1993), 2128-2154.

T. Glimm, D. Headon and M.A. Kiskowski. Computational and mathematical models of chondrogenesis in vertebrate limbs. Birth Defects Res C Embryo Today, 96(2012), 176-92.

J. Gros, J.K. Hu, C. Vineqoni, P.F. Feruglio, R. Weissleder and C.J. Tabin. WNT5A/JNK and FGF/MAPK pathways regulate the cellular events shaping the vertebrate limb bud. Curr Biol, 20(2010), 1993-2002.

B. D. Harfe, P. J. Scherz, S. Nissim, H. Tian, A. P. McMahon and C. J. Tabin, Evidence for an expansion-based temporal Shh gradient in specifying vertebrate digit identities. Cell, 118(2004), 517-528.

H. G. E. Hentschel, T. Glimm, J. A. Glazier, S. A. Newman. Dynamical mechanisms for skeletal pattern formation in the vertebrate limb. Proc. R. Soc. B, 271 (2004), 1713 --1722.

J. R. Hinchliffe, Developmental basis of limb evolution. Int J Dev Biol, 46 (2002), 835-845.

T. Hirashima, Y. Iwasa and Y. Morishita, Distance between AER and ZPA is defined by feed-forward loop and is stabilized by their feedback loop in vertebrate limb bud, Bull. Math. Biol., 70(2008), 438-459.

S. Hopyan, J. Sharpe, and Y. Yang, Budding Behaviors: Growth of the Limb as a Model of Morphogenesis, Dev Dyn, 240 (2011), 1054-62.

W. Hundsdorfer. Trapezoidal and midpoint splittings for initial-boundary value problems. Mathematics of Computation, 67 (1998), 1047-1062.

J.A. Izaguirre, R. Chaturvedi, C. Huang, T. Cickovski, J. Coffland, G. Thomas, G. Forgacs, M. Alber, G. Hentschel, S.A. Newman, and J. A. Glazier, CompuCell, a multi-model framework for simulation of morphogenesis, Bioinformatics, 20 (7) (2004), 1129-1137.

M. A. Kiskowski, M. S. Alber, G. L. Thomas, J. A. Glazier, N. B. Bronstein, J. Pu and

S. A. Newman, Interplay between activator-inhibitor coupling and cell-matrix adhesion in a cellular automaton model for chondrogenic patterning. Dev Biol, 271 (2004), 372-387.

E. Klopocki, C. E. Ott, N. Benatar, R. Ullmann, S. Mundlos and K. Lehmann, A microduplication of the long range SHH limb regulator (ZRS) is associated with triphalangeal thumb-polysyndactyly syndrome. J Med Genet, 45(2008), 370-375.

S. Kondo and T. Miura, Reaction-diffusion model as a framework for understanding biological pattern formation. Science, 329(2010), 1616-1620.

R.A. Kosher, M.P. Savage and S.C. Chan. In vitro studies on the morphogenesis and differentiation of the mesoderm subjacent to the apical ectodermal ridge of the embryonic chick limb-bud. J. Embryol Exp Morphol. 50 (1979), 75 – 97.

P. K. Kundu. *Fluid Mechanics.* Academic Press, Inc, London, (1990).

E. Laufer, C.E. Nelson, R.L. Johnson, B.A. Morgan and C. Tabin. Sonic hedgehog and Fgf-4 act through a signaling cascade and feedback loop to integrate growth and patterning of the developing limb bud. Cell, 79(1994), 993-1003.

C.M. Leonard, H.M. Fuld, D.A. Frenz, S.A. Downie, J. Massagué, S.A. Newman. Role of transforming growth factor-β in chondrogenic pattern formation in the embryonic limb: stimulation of mesenchymal condensation and fibronectin gene expression by exogenenous TGF-β and evidence for endogenous TGF-β-like activity. Dev Biol., 145(1991), 99-109.

S. Li and K. Muneoka. Cell migration and chick limb development: chemotactic action of FGF-4 and the AER. Dev Biol. 211 (1999), 335-47.

Y. Litingtung, R. D. Dahn, Y. Li, J. F. Fallon and C. Chiang. Shh and Gli3 are dispensable for limb skeleton formation but regulate digit number and identity. Nature, 418(2002), 979-83.

A. Madzvamuse, A.J. Wathen, P.K. Maini. A moving grid finite element method applied to a model biological pattern generator. Journal of Computational Physics, 190 (2003), 478 -- 500.

A. Madzvamuse, P.K. Maini, A.J. Wathen. A moving grid finite element method for the simulation of pattern generation by Turing models on growing domains. J. Sci. Comput., 24 (2005), 247- 262.

T. Mammoto, A. Mammoto, Y. S. Torisawa, T. Tat, A. Gibbs, R. Derda, R. Mannix, M. de Bruijn, C. W. Yung, D. Huh and D. E. Ingber, Mechanochemical control of mesenchymal condensation and embryonic tooth organ formation. Dev Cell, 21(2011), 758-769.

F.V. Mariani, G. R. Martin. Deciphering skeletal patterning: clues from the limb. Nature, 423(2003), 319-25.

P. Martin and J. Lewis. Normal development of the skeleton in chick limb buds devoid of dorsal ectoderm. Dev Biol, 118 (1986), 233-46.

H. Meinhardt. Models for the ontogenetic development of higher organisms. Rev

Physiol Biochem Pharmacol, 80 (1978), 47-104.

H. Meinhardt, Models of Biological Pattern Formation (1982), London: Academic Press.

H. Meinhardt, A boundary model for pattern formation in vertebrate limbs, J. Embryol. Exp. Morphol., 76(1983), 115-137.

H. Meinhardt and A. Gierer. Pattern formation by local self-activation and lateral inhibition. Bioessays. 22(2000), 753-60.

H. Meinhardt. Models of biological pattern formation: from elementary steps to the organization of embryonic axes. Curr Top Dev Biol. 81(2008), 1-63.

T. Miura and P. K. Maini, Speed of pattern appearance in reaction-diffusion models: implications in the pattern formation of limb bud mesenchyme cells. Bull Math Biol, 66 (2004), 627-649.

T. Miura, K. Shiota. TGFβ2 acts as an "activator" molecule in reaction-diffusion model and is involved in cell sorting phenomenon in mouse limb micromass culture. Dev Dyn. 217(2000a), 241-9.

T. Miura and K. Shiota, Extracellular matrix environment influences chondrogenic pattern formation in limb bud micromass culture: Experimental verification of theoretical models. Anat Rec, 258(2000b), 100-107.

T. Miura, K. Shiota, G. Morriss-Kay and P. K. Maini, Mixed-mode pattern in Doublefoot mutant mouse limb--Turing reaction-diffusion model on a growing domain during limb development. J Theor Biol, 240(2006), 562-573.

M. Z. Moftah, S. A. Downie, N. B. Bronstein, N. Mezentseva, J. Pu, P.A. Maher, S.A. Newman. Ectodermal FGFs induce perinodular inhibition of limb chondrogenesis in vitro and in vivo via FGF receptor 2. Dev Biol. 249(2002), 270-82.

Y. Morishita and Y. Iwasa, Growth based morphogenesis of vertebrate limb bud, Bulletin of Mathematical Biology, 70(2008), 1957-1978.

C.M. Murea and H. G. E. Hentschel, A finite element method for growth in biological development, Math. Biosci. Engineering. 4(2007), 339-353.

J. D. Murray, Mathematical biology, Springer, New York (2002).

C.E. Nelson, B. A. Morgan, A.C. Burke, E. Laufer, E. DiMambro, L.C. Murtaugh, E. Gonzales, L. Tessarollo, L. F. Parada, C. Tabin. Analysis of Hox gene expression in the chick limb bud.   Development, 122 (1996), 1449 -- 1466.

S.A. Newman, G. B. Müller. Origination and innovation in the vertebrate limb skeleton: an epigenetic perspective. J. Exp. Zoolog. B Mol. Dev. Evol. 304 (2005), 593--609.

S.A. Newman, R. Bhat. Activator-inhibitor dynamics of vertebrate limb pattern formation. Birth Defects Res C Embryo Today, 81 (2007), 305--319.

S.A. Newman, S.Christley, T.Glimm, H.G.E. Hentschel, B. Kazmierczak, Y.-T. Zhang, J. Zhu and M. Alber, Multiscale models for vertebrate limb development, Current Topics in Developmental Biology, 81(2008), 311-340.

S. A. Newman, G. Forgacs and G. B. Müller, Before programs: The physical origination of multicellular forms. Int. J. Dev. Biol., 50(2006), 289-299.

S.A. Newman, H. L. Frisch. Dynamics of skeletal pattern formation in developing chick

limb. Science, 205 (1979), 662-668.

L. Niswander, S. Jeffrey, G.R. Martin, C. Tickle. A positive feedback loop coordinates growth and patterning in the vertebrate limb. Nature. 371(1994), 609-12.

S.A. Oberlender and R.S. Tuan. Expression and functional involvement of N-cadherin in embryonic limb chondrogenesis. Development. 120(1994), 177-87.

D.M. Ornitz, P.J. Marie. FGF signaling pathways in endochondral and intramembranous bone development and human genetic disease. Genes Dev. 16(2002), 1446-65.

G. F. Oster, J. D. Murray and A. K. Harris, Mechanical aspects of mesenchymal morphogenesis. J. Embryol. Exp. Morphol., 78(1983), 83-125.

C.S. Peskin, The immersed boundary method, Acta Numerica, 11(2002), 1–39.

N.J. Poplawski, M. Swat, J.S. Gens and J.A. Glazier, Adhesion between cells, diffusion of growth factors, and elasticity of the AER produce the paddle shape of the chick limb. Physica A, 373 (2007), 521-532.

K. G. Peters, S. Werner, G. Chen and L. T. Williams, Two FGF receptor genes are differentially expressed in epithelial and mesenchymal tissues during limb formation and organogenesis in the mouse. Development, 114(1992), 233-243.

W.H. Reed and T.R. Hill, Triangular mesh methods for neutron transport equation. Tech. Report LA-UR-73-479, Los Alamos Scientific Laboratory, (1973).

B. Rivière. *Discontinuous Galerkin Methods for Solving Elliptic and Parabolic Equations.* SIAM, (2008).

M.A. Ros, G.E. Lyons, S. Mackem and J.F. Fallon. Recombinant limbs as a model to study homeobox gene regulation during limb development. Dev. Biol., 166(1994), 59-72.

I. Salazar-Ciudad and J. Jernvall, Graduality and innovation in the evolution of complex phenotypes: insights from development. J Exp Zool B (Mol Dev Evol), (2005).

I. Salazar-Ciudad and J. Jernvall, A computational model of teeth and the developmental origins of morphological variation. Nature, 464(2010), 583-586.

I. Salazar-Ciudad, J. Jernvall and S. A. Newman Mechanisms of pattern formation in development and evolution. Development, 130(2003), 2027-2037.

S. Schnell, P.K. Maini, S.A. Newman, T.J. Newman (Eds.), *Multiscale Modeling of Developmental Systems*, Current Topics in Developmental Biology, 81(2008), 1-539.

J.W. Jr. Saunders. The proximo-distal sequence of origin of the parts of the chick wing and the role of the ectoderm. J Exp Zool, 108(1948), 363-402.

M. Scianna, L. Preziosi, *Cellular Potts Models: Multiscale Extensions and Biological Applications*, Chapman & Hall/CRC Mathematical & Computational Biology (2013).

N. Shubin, C. Tabin, S. Carroll. Deep homology and the origins of evolutionary novelty. Nature, 457 (2009), 818 – 823.

D. Stopak and A. K. Harris, Connective tissue morphogenesis by fibroblast traction. I. Tissue culture observations. Develop. Biol., 90(1982), 383-398.

G. Strang, On the construction and comparison of difference schemes, *SIAM J. Numer.*

Anal. 8(1968), 506-517.

D. Summerbell. A descriptive study of the rate of elongation and differentiation of the skeleton of the developing chick wing. J. Embryol. Exp. Morphol., 35 (1976), 241--260.

D. Summerbell, J.H. Lewis, L. Wolpert. Positional information in chick limb morphogenesis. Nature, 244 (1973), 492 - 496.

M. Sun, F. Ma, X. Zeng, Q. Liu, X. L. Zhao, F. X. Wu, G. P. Wu, Z. F. Zhang, B. Gu, Y. F. Zhao, S. H. Tian, B. Lin, X. Y. Kong, X. L. Zhang, W. Yang, W. H. Lo and X. Zhang. Triphalangeal thumb-polysyndactyly syndrome and syndactyly type IV are caused by genomic duplications involving the long range, limb-specific SHH enhancer. J Med Genet, 45(2008), 589-595.

X. Sun, F. V. Mariani and G. R. Martin, Functions of FGF signalling from the apical ectodermal ridge in limb development. Nature, 418(2002), 501-508.

T. Svingen, K. F. Tonissen. Hox transcription factors and their elusive mammalian gene targets. Heredity, 97 (2006), 88 -- 96.

G. Szebenyi, M.P. Savage, B.B. Olwin, J.F. Fallon. Changes in the expression of fibroblast growth factor receptors mark distinct stages of chondrogenesis in vitro and during chick limb skeletal patterning. Dev Dyn. 204(1995), 446-56.

C. Tickle. Patterning systems - from one end of the limb to the other. Dev. Cell, 4 (2003), 449--458.

C. Tickle, D. Summerbell, L. Wolpert. Positional signalling and specification of digits in chick limb morphogenesis. Nature. 254(1975), 199-202.

M. Towers and C. Tickle. Generation of pattern and form in the developing limb. Int. J. Dev. Biol., 53 (2009), 805-812.

M. Towers, L. Wolpert and C. Tickle, Gradients of signalling in the developing limb. Curr Opin Cell Biol, 24(2012), 181-187.

P.A. Tsonis, K. Del Rio-Tsonis, J.L. Millan, M.J. Wheelock. Expression of N-cadherin and alkaline phosphatase in chick limb bud mesenchymal cells: regulation by 1,25-dihydroxyvitamin D3 or TGF-β 1. Exp Cell Res. 213(1994), 433-7.

R.B. Widelitz, T.X. Jiang, B.A. Murray and C.M. Chuong. Adhesion molecules in skeletogenesis: II. Neural cell adhesion molecules mediate precartilaginous mesenchymal condensations and enhance chondrogenesis. J Cell Physiol. 156(1993), 399-411.

D. Wieczorek, B. Pawlik, Y. Li, N. A. Akarsu, A. Caliebe, K. J. May, B. Schweiger, F. R. Vargas, S. Balci, G. Gillessen-Kaesbach and B. Wollnik, A specific mutation in the distant sonic hedgehog (SHH) cis-regulator (ZRS) causes Werner mesomelic syndrome (WMS) while complete ZRS duplications underlie Haas type polysyndactyly and preaxial polydactyly (PPD) with or without triphalangeal thumb. Hum Mutat, 31(2010), 81-89.

L. Wolpert. Positional information and the spatial pattern of cellular differentiation. J. Theor Biol. 25 (1969), 1-47.

L. Wolpert. Positional information and pattern formation. Curr Topics Dev Biol. 6 (1971), 183-224.

L. Wolpert and A. Hornbruch, Double anterior chick limb buds and models for

cartilage rudiment specification. Development, 109(1990), 961-966.

L. A. Wyngaarden, K. M. Vogeli, B. G. Ciruna, M. Wells, A. K. Hadjantonakis, and S. Hopyan, Oriented cell motility and division underlie early limb bud morphogenesis, Development, 137 (2010), 2551-8.

O.K. Wilby and D.A. Ede, A model generating the pattern of cartilage skeletal elements in the embryonic chick limb, J. Theor. Biol. 52(1975), 199-217.

Z. Xu, O. Kim, M. Kamocka, E.D. Rosen and M. Alber, Multiscale Models of Thrombogenesis , Wiley Interdiscip Rev Syst Biol Med. 4(2012), 237-46.

Y. Yang and L. Niswander. Interaction between the signaling molecules WNT7a and SHH during vertebrate limb development: dorsal signals regulate anteroposterior patterning. Cell, 80(1995), 939-47.

E.A. Zamir, A. Czirok, C. Cui, C.D. Little and B.J. Rongish. Mesodermal cell displacements during avian gastrulation are due to both individual cell-autonomous and convective tissue movements. Proc Natl Acad Sci USA. 103 (2006), 19806-11.

R. Zeller, J. Lopez-Rios and A. Zuniga. Vertebrate limb bud development: moving towards integrative analysis of organogenesis. Nat Rev Genet, 10(2009), 845-58.

J. Zhu, Y.-T. Zhang, S.A. Newman, M.S. Alber. Application of discontinuous Galerkin methods for reaction-diffusion systems in developmental biology. Journal of Scientific Computing, 40 (2009a), 391 – 418.

J. Zhu, Y.-T. Zhang, S.A. Newman, M.S. Alber. A finite element model based on discontinuous Galerkin methods on moving grids for vertebrate limb pattern formation. Mathematical Modelling of Natural Phenomena, 4 (2009b), 131 – 148.

J. Zhu, Y.-T. Zhang, M. S. Alber, S. A. Newman. Bare bones pattern formation: a core regulatory network in varying geometries reproduces major features of vertebrate limb development and evolution, PLoS One, 5(2010), e10892.

Figure Legends

Fig. 1. Development of a representative vertebrate limb (a chicken forelimb). The limb bud at successive stages is shown as if transparent and its outgrowth and shaping and the progress of chondrogenesis within it are both shown. The lighter gray regions represent precartilage; the darker-gray regions represent definitive cartilage. The single proximal element that forms first is the humerus (the femur in the leg); the two elements of the mid-wing form next, the radius and the ulna (the tibia and fibula in the leg); the distal-most, last-forming, elements are the digits. Below, the proximodistal, anteroposterior, and dorsoventral axes are indicated on an illustration of a human hand. (Modified from Forgacs and Newman, 2005).

Fig. 2. Results of computational optimization of a finite-element model for limb bud shaping.. (Slightly modified from Boehm et al., 2011)   Limb orientations are as shown in Fig. 1.

Fig. 3. Computational and experimental Patched (Ptc) responses to Sonic hedgehog (Shh) bead implants (upper panels) and ZPA tissue implants (lower panels). (*Upper*) Numerical simulations of Ptc concentration 2, 6, and 18 h after bead implants (*A*, *C*, and *E*, respectively). (*Lower*) Ptc concentration 12, 16, and 20 h after tissue implant (*A*, *C*, and *E*, respectively). Experimental results are from Drossopoulou et al. (2000) for *ptc* transcript expression 2, 6, and 16 h post-bead implants and for ZPA grafts, 4, 8, and 16 h post-implant (*B*, *D*, and *F*, respectively). The figures for numerical simulations were rescaled. (From Dillon et al., 2003).

Fig, 4. Schematic representation of the biochemical genetic circuitry underlying the pattern-forming instability described in the model of Hentschel *et al.* (2004), superimposed on a two-dimensional representation of the 5-day limb bud. The colored rectangles represent the distribution of the densities of the cell types designated in the model, defined by the expression of the various FGF receptors in the different zones. The apical zone contains a high density of cells expressing FGFR1 (green). In this

1

zone, cell rearrangement is suppressed by the FGFs emanating from the AER. The active zone is the site of the spatiotemporal regulation of mesenchymal cell condensation. Pattern formation begins with the establishment of populations of cells expressing FGF receptor 2 (red). The lower part of the figure gives an enlarged version of part of this zone. The curved arrows indicate the positively autoregulatory (i.e., TGF-β); the straight lines ending in circles indicate the laterally acting inhibitor. When condensed cells leave the proximal end of the active zone and enter the frozen zone they differentiate into cartilage cells, which express FGFR3 (blue), and their spatiotemporal pattern becomes fixed. At different stages of development the active zone will contain different numbers of elements; eventually the frozen zone will encompass the entire pattern. The length of the dorsoventral axis (normal to the plane of the figure; see Fig. 8.13) is collapsed to zero in this simplified model. PD, proximodistal axis; AP, anteroposterior axis. (Based on Hentschel et al., 2004; figure modified from Forgacs and Newman, 2005.)

Fig. 5. Sequential generation of morphogen and condensation patterns in two multiscale 3D simulations of limb development based on the model of Hentschel et al. (2004). (A) Time series of the concentration of the diffusible morphogen TGF-β displayed in cross-sections of the active zone (per Hentschel et al., 2004) of the chick limb at successive stages of development, with time increasing in the upward direction (Chaturvedi et al., 2005). (B) A three-dimensional simulation of mesenchymal cell distribution during chick limb development. Cells that have undergone condensation are shown in gray (Cickovski et al., 2005). Whereas the cell density was represented as a continuous variable in Hentschel et al. (2004), both of these studies employed the Cellular Potts Model (Glazier and Graner, 1993) to represent cell position and motion (though only the morphogen profile is shown in (A). In each study simulations were performed using the CompuCell3D multimodel simulation framework (http://www.compucell3d.org/). (Panel A from Chaturvedi (2005). Panel B, slightly modified from Cickovski et al.,2005, from Forgacs and Newman, 2005).

Fig. 6. Simulations of AER removal with the model of Zhu et al. (2010). (Left two columns) Drawings of AER removal experiments, based on Saunders (1948). The top images show an intact chicken wing bud at an early stage of development and the limb skeleton that it generates. The middle images show a wing bud at the same early stage with the AER removed, and the resulting limb skeleton, which attains a normal size but is truncated beginning at the elbow. The bottom images show a later-stage wing bud the AER of which has been removed. The resulting skeleton is truncated from the wrist onward. (Right column): Top: AER (e.g., suppressive morphogen source) left intact; normal development results. Middle: AER deleted early during the simulation. Bottom: AER deleted later during the simulation. The same parameters were used in all three simulations and all simulated limbs were allowed to develop for the same time. (From Zhu et al., 2010).

Fig. 7. Simulation of fossil limb skeletons with the model of Zhu et al. (2010). Hypothetical developmental scenarios were used, as described in the text and the original paper. The end-stages of the simulations of the ichthyosaur *Brachypterygius*, two lobe-finned fish, *Sauripterus* and *Eusthenopteron*, and two forms that are transitional between those organisms and amphibians, *Panderichthys* and *Tiktaalik*, are shown on the right. See Zhu et al. (2010) for the sources of the fossil drawings and details of the simulations.

Fig. 8. Mechanism by which the loss of a middle finger can occur in the heuristic model of limb development of Glimm et al (2012). As the external morphogen gradient becomes less steep, the local activator concentration at the second peak falls below the threshold concentration. The panels on the left show schematic plots of the corresponding spatially dependent kinetics terms. In the center panels, the corresponding steady state activator concentrations are shown. The right-hand side shows the patterns induced in those regions where the activator concentration is above the threshold. Thus, the dark bars represent precartilage condensations, the precursors to the digits. While all 5 digits appear in the first four rows (with variations in thickness resulting from the effect of the orthogonal modifying gradient), in the fifth row there are only 4 digits; a middle digit is "lost" (i.e., fails to form). In the panels on the right, the horizontal direction is the anteroposterior axis, and the vertical direction proximodistal axis. (From Glimm et al., 2012).
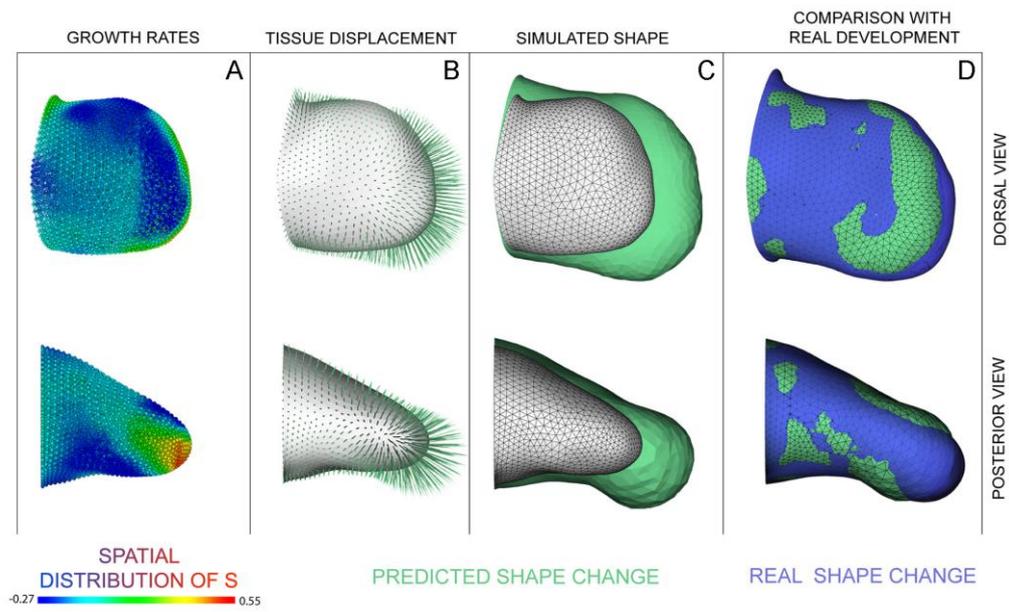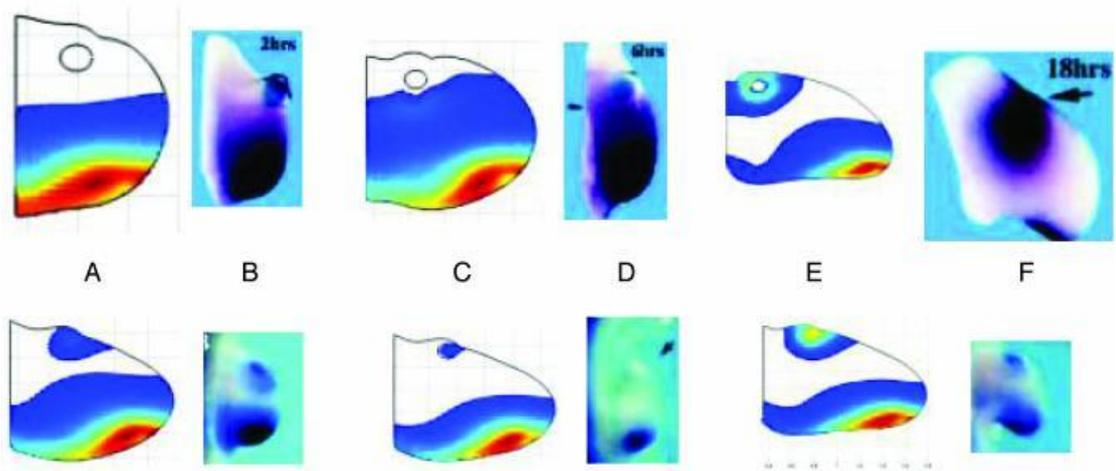
Fig. 1

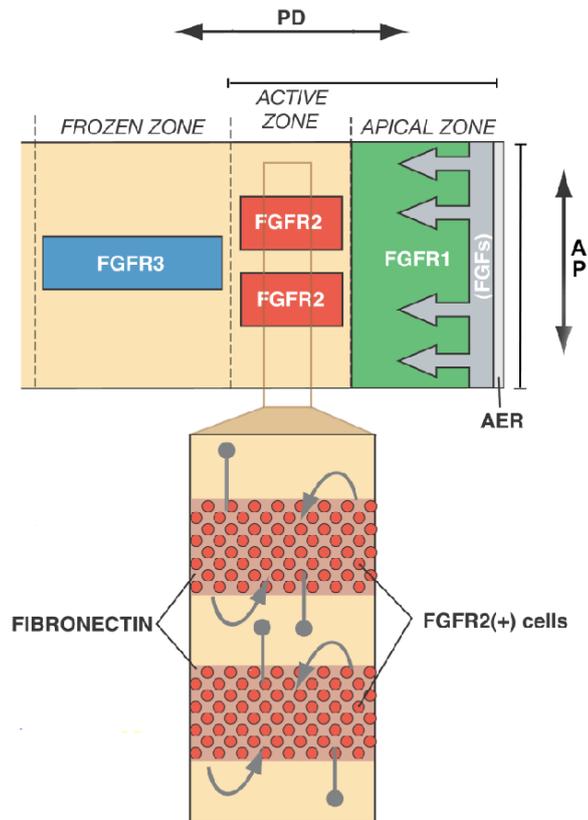GROWTH RATES   TISSUE DISPLACEMENT   SIMULATED SHAPE   COMPARISON WITH REAL DEVELOPMENT

A   B   C   D

DORSAL VIEW

POSTERIOR VIEW

SPATIAL DISTRIBUTION OF S

-0.27   0.55

PREDICTED SHAPE CHANGE

REAL SHAPE CHANGE

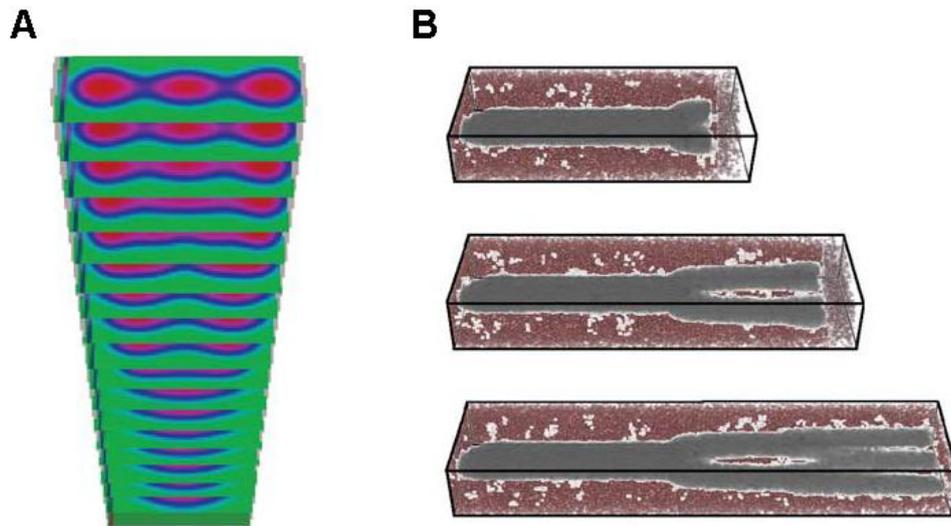Fig. 2

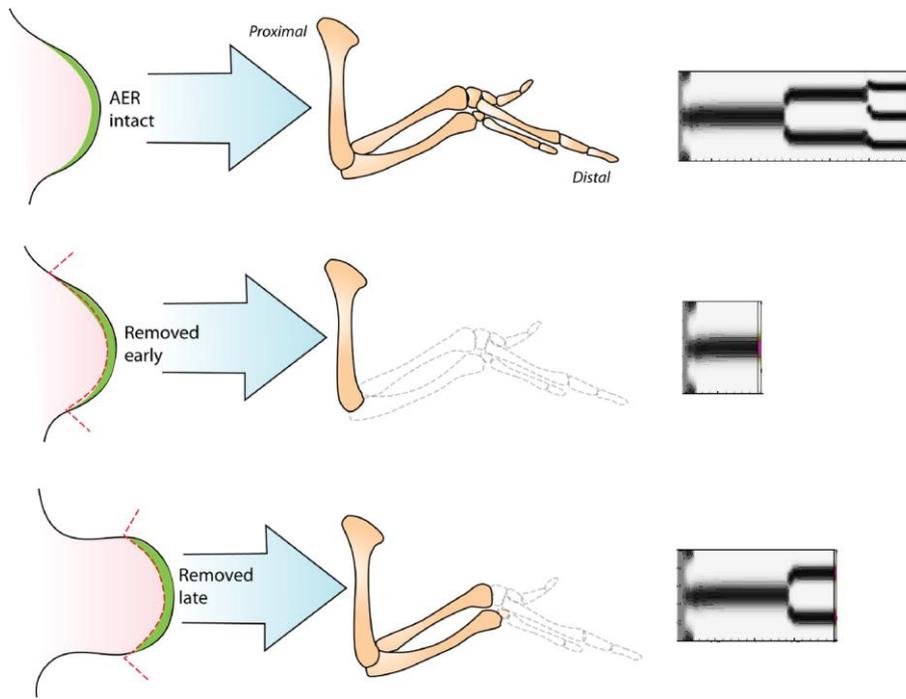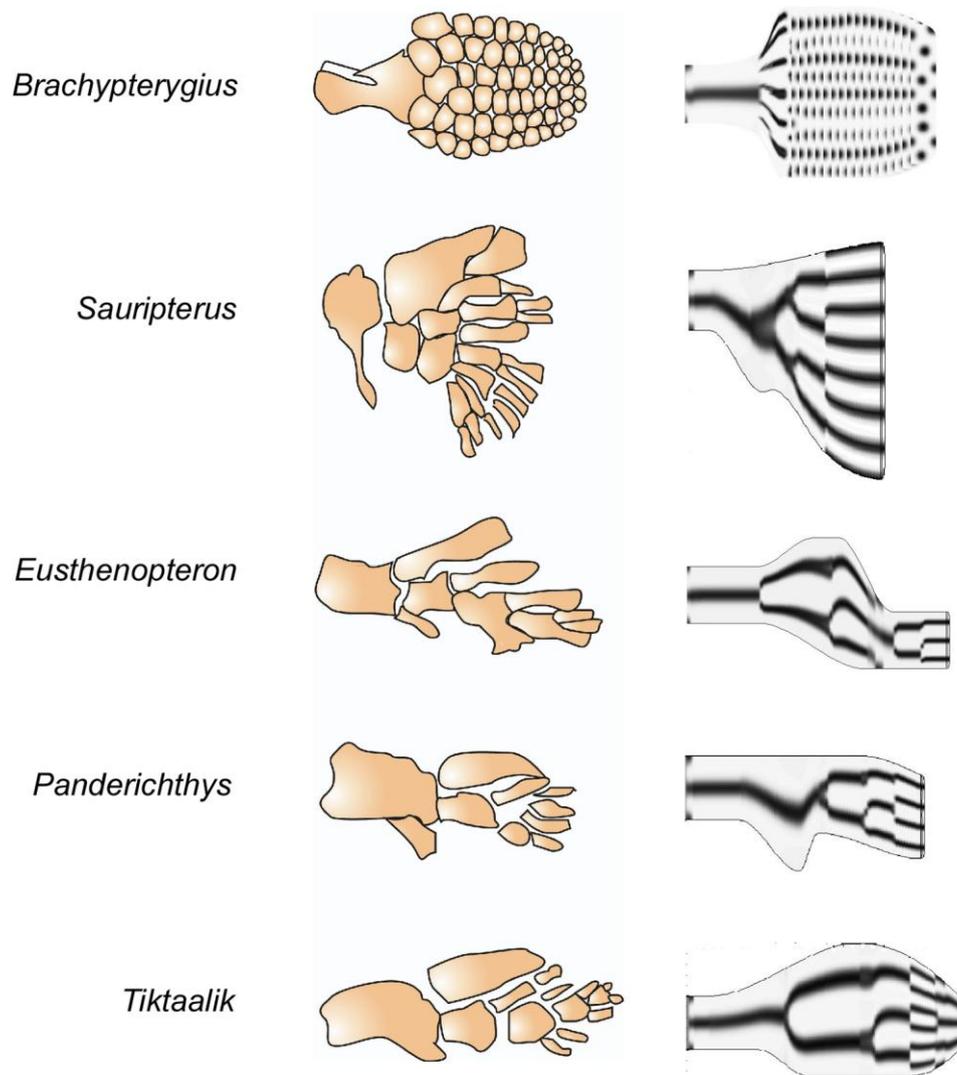A   B   C   D   E   F
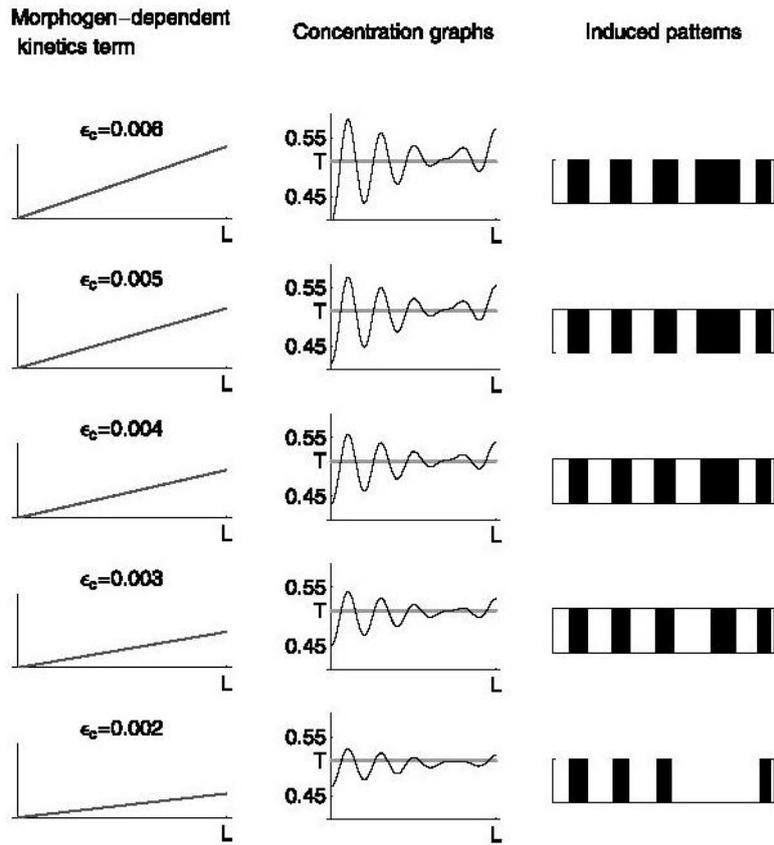
Fig. 3

Fig. 4

A

B
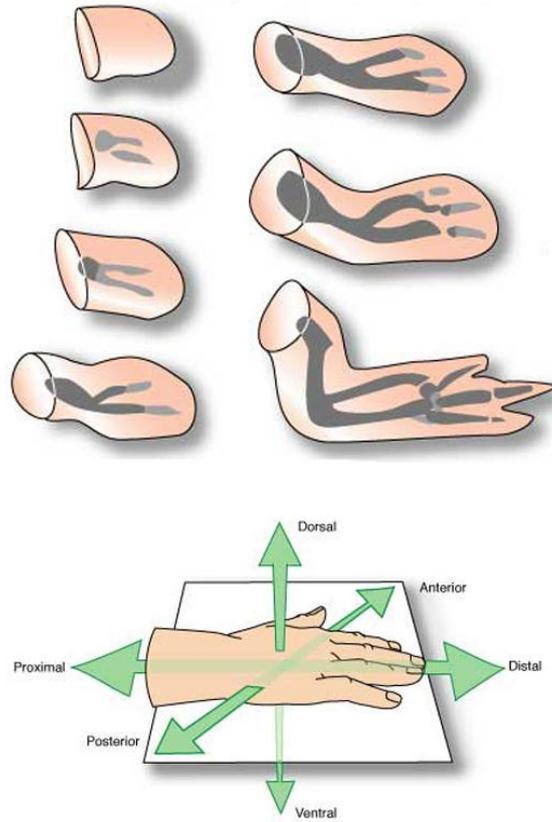
Fig. 5

Fig. 6

Fig. 7

Fig. 8

Highlights

- We review major mathematical and computational models of vertebrate limb development.

- Models cover limb bud outgrowth and shaping, gradient formation, and skeletogenesis.

- Models help explain microsurgical experiments, mutations, and evolution of the limb.

- Multiscale mathematical modeling is now central to the study of limb morphogenesis.